



HAL
open science

Integrated metabolomic, molecular networking, and genome mining analyses uncover novel angucyclines from *Streptomyces* sp. RO-S4 strain isolated from Bejaia Bay, Algeria

Rima Ouchene, Didier Stien, Juliette Segret, Mouloud Kecha, Alice Rodrigues, Carole Veckerlé, Marcelino Suzuki

► To cite this version:

Rima Ouchene, Didier Stien, Juliette Segret, Mouloud Kecha, Alice Rodrigues, et al.. Integrated metabolomic, molecular networking, and genome mining analyses uncover novel angucyclines from *Streptomyces* sp. RO-S4 strain isolated from Bejaia Bay, Algeria. 2022. hal-03746686v1

HAL Id: hal-03746686

<https://hal.sorbonne-universite.fr/hal-03746686v1>

Preprint submitted on 4 Oct 2022 (v1), last revised 5 Aug 2022 (v2)

HAL is a multi-disciplinary open access archive for the deposit and dissemination of scientific research documents, whether they are published or not. The documents may come from teaching and research institutions in France or abroad, or from public or private research centers.

L'archive ouverte pluridisciplinaire **HAL**, est destinée au dépôt et à la diffusion de documents scientifiques de niveau recherche, publiés ou non, émanant des établissements d'enseignement et de recherche français ou étrangers, des laboratoires publics ou privés.

1 **Integrated metabolomic, molecular networking, and genome mining**
2 **analyses uncover novel angucyclines from *Streptomyces* sp. RO-S4 strain**
3 **isolated from Bejaia Bay, Algeria**

4
5 **Rima Ouchene^{1,2}, Didier Stien^{2*}, Juliette Segret², Mouloud Kecha¹, Alice M. S. Rodrigues²,**
6 **Carole Veckerlé², Marcelino T. Suzuki^{2*}**

7
8 ¹Laboratoire de Microbiologie Appliquée (LMA), Faculté des Sciences de la Nature et de la
9 Vie, Université de Bejaia, 06000 Bejaia, Algérie.

10 ²Sorbonne Université, CNRS, Laboratoire de Biodiversité et Biotechnologies Microbiennes,
11 LBBM, Observatoire Océanologique, F-66650, Banyuls-sur-mer, France.

12
13
14 *Corresponding authors: Didier Stien (didier.stien@cnrs.fr), Marcelino T. Suzuki
15 (suzuki@obs-banyuls.fr).

16 **Key words:** Marine *Streptomyces*, Antibacterial activity, MRSA, Metabolomic analysis,
17 Molecular Networking, Genome mining.

18
19

20 **Abstract**

21 Multi-omic approaches have recently made big strides towards the effective exploration of
22 microorganisms and accelerating the discovery of new bioactive compounds. We combined
23 metabolomic, molecular networking, and genomic-based approaches to investigate the
24 metabolic potential of the *Streptomyces* sp. RO-S4 strain isolated from the polluted waters of
25 Bejaia Bay in Algeria. Antagonistic assays against *methicillin-resistant Staphylococcus aureus*
26 with RO-S4 organic extracts showed an inhibition zone of 20 mm by the agar diffusion method,
27 and its minimum inhibitory concentration was 16 µg/mL. A molecular network was created
28 using GNPS and annotated through the comparison of MS/MS spectra against several
29 databases. The predominant compounds in the RO-S4 extract belonged to the angucyclines
30 family. Three compounds were annotated as known metabolites, while all the others were
31 putatively new to Science. Notably, all compounds had fridamycin-like aglycones, and several
32 of them had a lactonized D ring analogous to that of urdamycin L. The whole genome of
33 *Streptomyces* RO-S4 was sequenced to identify the biosynthetic gene cluster (BGC) encoding
34 for these angucyclines, which yielded a draft genome of 7,497,846 bp with 72.4% G+C content.
35 Subsequently, a genome mining analysis revealed 19 putative biosynthetic gene clusters,
36 including a grincamycin-like BGC with a high similarity to that of *Streptomyces* sp. CZN-748
37 previously reported to also produce mostly open fridamycin-like aglycones. As the ring-
38 opening process leading to these compounds is still not defined, we performed comparative
39 analysis with other angucycline BGCs and advanced some hypotheses to explain the ring-
40 opening and lactone formation, possibly linked to the uncoupling between the activity of GcnE
41 and GcnM homologues in the RO-S4 strain. The combination of metabolomic and genomic
42 approaches greatly improved the interpretation of the metabolic potential of the RO-S4 strain.

43

44 **Introduction**

45 The emergence of novel mechanisms of antimicrobial resistance is increasing and spreading
46 worldwide, posing a challenge to mankind. The World Health Organization has stated that
47 antibiotic resistance will be one of the biggest threats to human health in the future¹. Multidrug-
48 resistant organisms have become common not only in hospital settings but also in the wide
49 community settings, suggesting that reservoirs of antibiotic-resistant bacteria are present
50 outside hospitals (reviewed by Munita and Arias)². This antibiotic resistance crisis has been
51 attributed to overuse and inappropriate use of these drugs, as well as the lack of antimicrobial
52 drug development by the pharmaceutical industry due to reduced economic incentives and
53 difficult regulatory requirements^{3,4}. Methicillin-resistant *Staphylococcus aureus* (MRSA) is the
54 most common cause of nosocomial infections as it is very capable of developing antibiotic
55 resistance^{5,6}. Many challenges are faced by laboratories and clinicians in the diagnosis and
56 treatment of MRSA infections, some of which were highlighted by Edwards and coworkers⁷. It
57 is thus clear that the search for new bioactive compounds to combat antimicrobial resistance is
58 a research priority.

59 Marine environments represent a largely unexplored source for the isolation of new
60 microorganisms⁸. They display a unique combination of environmental conditions and
61 organisms with distinct metabolic capabilities to adapt and thrive^{9,10}. A large number of
62 bioactive compounds have been isolated from marine organisms^{11,12,13}, particularly
63 Actinobacteria, which have been a main source of natural products in the past^{14,15,16}. Among
64 the latter, the *Streptomyces* genus is well known for its ability to produce a wide range of
65 bioactive metabolites as well as antibacterial, anticancer, antifungal, antiparasitic, and
66 immunosuppressive agents^{17,18}, representing the most prolific source of bioactive metabolites
67 that have been approved for clinical use, notably as antibiotics¹⁹.

68 Traditionally, activity-guided fractionation of metabolite extracts, followed by purification and
69 characterization of metabolites, has commonly been used for natural product research, but this
70 approach often leads to the isolation of already known molecules. More recently, significant
71 developments in genetics, genomics, and data analysis have greatly changed natural product
72 research, leading to a new era in the emerging field of systems biology. Consequently, new
73 avenues were opened for the discovery of novel compounds from actinomycetes
74 (e.g.^{20,13,21,22,23,16}). Interestingly, metabolomics and genomics approaches have proven to be
75 efficient and promising tools for defining phenotypes in a dynamic context, with the potential
76 to reduce rediscovery rates^{24,25,26}, and several tools have been designed for this purpose, as
77 reported by Caesar and colleagues²⁷. These approaches have been successfully applied to study

78 the chemical diversity of marine bacteria and to uncover novel bioactive molecules^{28,29,30},
79 despite the challenges encountered due to the complexity of biological matrices³¹. More
80 recently, molecular networking, a tandem mass spectrometry (MS/MS) data organizational
81 approach, has been introduced in the field of drug discovery³², and the combination of system
82 analyses involving multi-omics data and genome-scale, metabolic network models has greatly
83 contributed to exploring bioactive Actinobacteria³³, and have great potential to accelerate
84 natural product discovery.

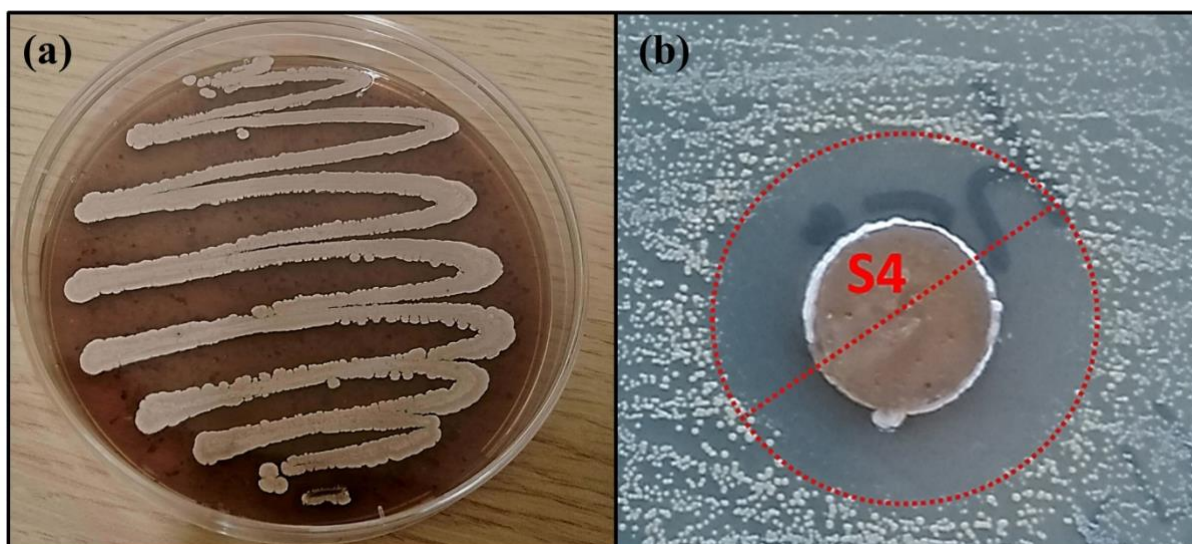
85 Here, we investigated the secreted metabolome of *Streptomyces* sp. RO-S4 in the quest for
86 novel antimicrobial compounds against antibiotic-multi-resistant *S. aureus* (MRSA). For this
87 purpose, we used a metabolomic approach based on ultra-performance high resolution tandem
88 mass spectrometry (UPLC-HRMS/MS) followed by the creation of a molecular network using
89 the Global Natural Product Social Molecular Networking (GNPS) analysis. These analyses
90 were combined with a genomic analysis to refine and further annotate the structural hypothesis
91 generated, and conversely, to understand the biosynthesis of the major angucyclines produced
92 by this strain.

93 **Results**

94 **Isolation and antimicrobial assays of the RO-S4 strain**

95 The RO-S4 strain was isolated from the bay of Bejaia City in Algeria. It grew well on the M2
96 medium, showing substrate growth typical for *Streptomyces* strains, with a brown powdery
97 aspect and producing a dark-brown pigment (Fig. 1a). Antimicrobial activity was first evaluated
98 against the MRSA strain by the agar diffusion method. It exhibited antagonistic activity against
99 this bacterium with an inhibition zone estimated at 20 mm (Fig. 1b). The 16S rRNA gene
100 sequence indicated that the strain belongs to the *Streptomyces* genus, with 99.79% identity to
101 *Streptomyces albogriseolus* NRRL B-1305 (T). The MIC of the ethyl acetate extract produced
102 by the RO-S4 strain was measured by the broth microdilution method on a 96-well plate. A
103 MIC value of 16 µg/mL was observed against the MRSA ATCC 43300 strain.

104



105

106 **Figure 1. (a):** The morphological appearance of *Streptomyces sp.* RO-S4 strain grown on M2
107 medium for 12 days at 28 °C. **(b):** MRSA inhibitory potential of the RO-S4 strain evaluated by
108 the agar diffusion method.

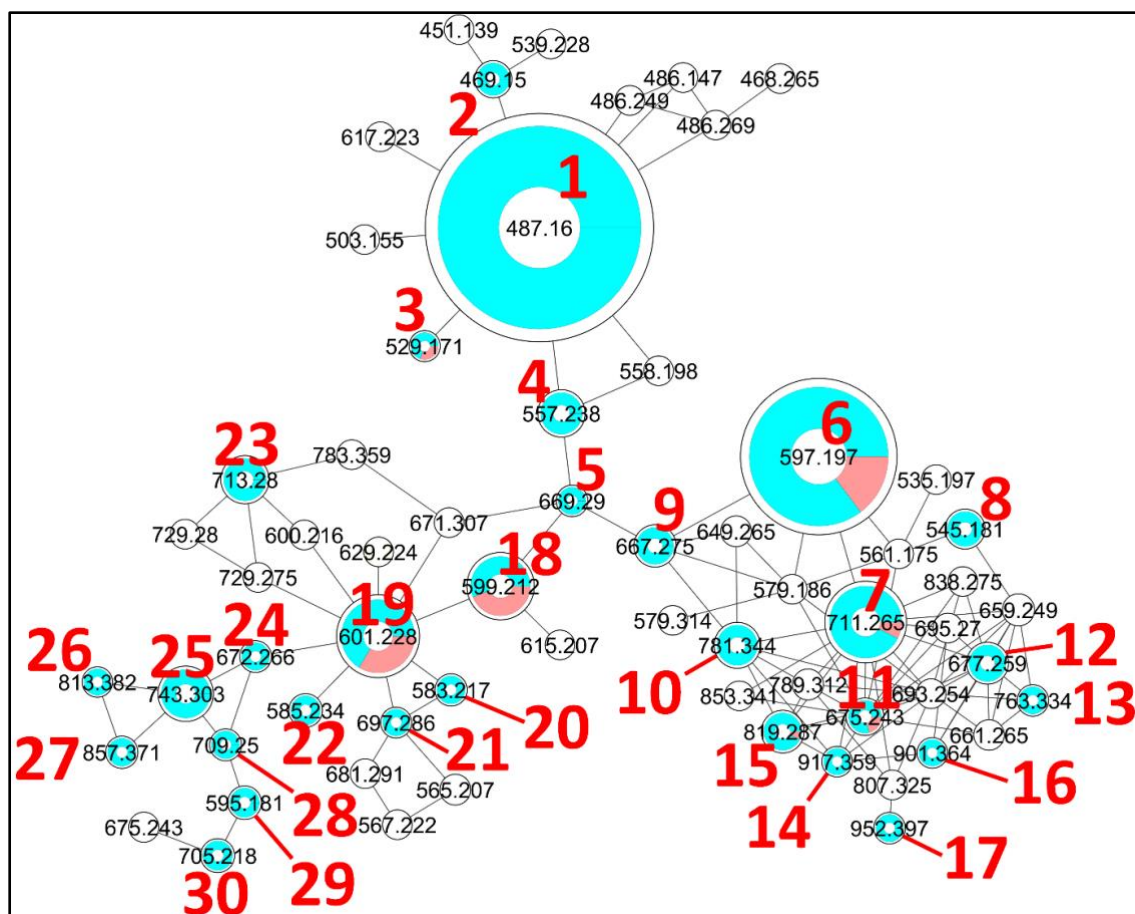
109 **Untargeted metabolomic analysis and Molecular Networking**

110 The metabolomic profile of the active ethyl acetate (EtOAc) crude extract was investigated
111 using UPLC-HRMS. An examination of the MS and collision induced MS/MS (MS² hereafter)
112 spectra of the main constituents of the mixture indicated that most metabolite molecular ions
113 fragmented to yield a product at m/z 487.1600 corresponding to the formula C₂₅H₂₇O₁₀⁺ (Calcd.
114 487.1599). The same ion was also detected as a protonated molecular ion corresponding to
115 compound **1** (Table 1). Compound **1** was annotated either as aquayamycin or as fridamycin A
116 or B by various dereplication tools. A comparison with experimental spectra from the MoNA
117 database confirmed that compound **1** was fridamycin A or its diastereomer fridamycin B. The
118 MS² spectra of fridamycin A and aquayamycin are very similar (Fig. S3, Supporting
119 Information). Nevertheless, two fragment ions are diagnostic. These are the ions at m/z 347.09
120 and 427.14, the relative intensities of which are very low in fridamycin A when compared to
121 those of aquayamycin.

122 As mentioned above, the [1+H]⁺ ion was also produced as a fragment resulting from in-source
123 fragmentation of many metabolites in the profile. The MS² spectra of all ions leading to a
124 487.1599 fragment clustered in the same node in the molecular network (MN). The MS²
125 spectrum obtained for the protonated molecular ion of compound **1** was compared to all other
126 MS² spectra of equimassic ions found whenever other more complex metabolites were

127 fragmented in source. The fragmentation patterns were all similar, confirming that many
128 metabolites in the MN were fridamycin A or B analogues. It was deduced that the strain
129 biosynthesizes the central fridamycin core and then adds various substituents to generate its
130 diverse products. Notably, the pentacyclic aquayamycin subunit was not detected in any of the
131 annotated metabolites. This observation was supported by the presence of a biosynthetic gene
132 cluster very close to that of *Streptomyces* sp. CNZ-748³⁴ which also produces a majority of
133 fridamycin-like compounds.

134 The parameters for MN were set to construct the best representative network containing all
135 fridamycin analogs (Fig. 2). The MN was constituted of three groups of ions. In the first group,
136 the annotation was propagated from **1** as follows. Compound **2** is a dehydrofridamycin based
137 on its molecular formula and MS² spectrum. Compound **3** molecular formula was C₂₇H₂₈O₁₁,
138 which might be annotated as an acetyl-fridamycin A or B, while the position of the acetyl group
139 could not be inferred from MS². Compound **4** whose molecular formula was C₃₀H₃₆O₁₀ (*m/z*
140 for [M+H]⁺ 669.2903, calcd. 669.2905) was a fridamycin bearing a C₅H₁₀ substituent. A
141 fridamycin isopentyl ester was thought to be a reasonable putative structure based on the
142 biosynthetic considerations below. Compound **5** could not be annotated more precisely than
143 just with its molecular formula, but its MS² spectrum is also one of a fridamycin analog. These
144 considerations indicated that **5** was new to Science.



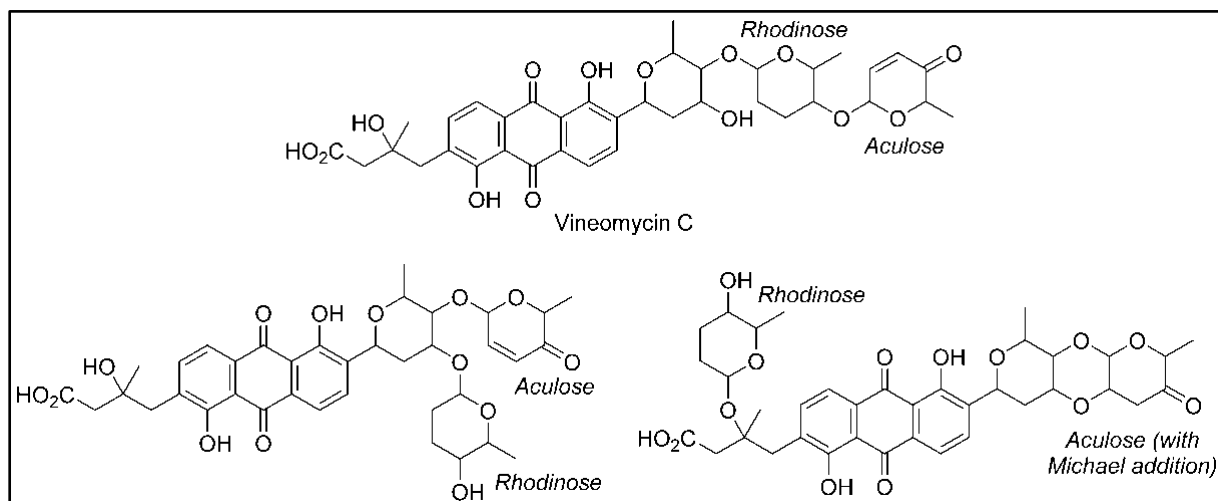
145

146 **Figure 2.** Molecular network generated with the GNPS Molecular Networking tool. The
147 diameter of the nodes represents the total extracted ion chromatogram integration of the
148 corresponding ion peak(s) and the blue/red pie chart represents the proportions of each isomer
149 in the cluster. The colorless nodes are clusters of MS² spectra of ions produced by in-source
150 fragmentation of diverse compounds and were thus neither annotated nor integrated
151 (integration was set to 0). Only protonated molecular ions were considered for integration
152 measurement.

153 In the second part of the fridamycin MN, compound **6a** protonated molecular ion was at *m/z*
154 597.1973, corresponding to the formula C₃₁H₃₃O₁₂⁺ (Calcd. *m/z* 597.1967). The formula and
155 fragmentation pattern were consistent with the annotation of **6a** as fridamycin D³⁵. Annotation
156 as fridamycin D was also supported by Sirius. An isomer of **6a** (**6b**) was also detected in smaller
157 relative proportions in the strain's metabolomic profile. Another major constituent of the strain
158 metabolome was compound **7a**, whose protonated molecular ion at *m/z* 711.2645, corresponded
159 to the formula C₃₇H₄₃O₁₄⁺ (Calcd. 711.2647). The molecular formula indicated that angucycline
160 **7a** may be vineomycin C³⁶. It was annotated as vineomycin C by Sirius as well, although with
161 57% confidence. In the collision-induced MS² spectrum of **7a** protonated molecular ion, the

162 rhodinose (or its distereoisomer amicetose) and the aculose oxonium ions were present at m/z
163 115.0756 and 111.0443 (Table S1), respectively, while the presence of the fridamycin A
164 aglycone was ascertained based on the common fridamycin A fragment ions (Fig. S16,
165 Supporting Information). Nonetheless, the first fragmentation steps in the MS² spectrum
166 suggested that the sugar sequence might be different to that of vineomycin C. The protonated
167 molecular ion lost both water (m/z for C₃₇H₄₁O₁₃⁺ 693.2258) and a C₆H₁₂O₃ group (m/z for
168 C₃₁H₃₁O₁₁⁺ 597.1938) which could only be assigned to the rhodinose/amicetose moiety. Hence,
169 the rhodinose could not be placed in between the aglycone and the aculose, as in vineomycin
170 C, and compound **7a** must be considered new to Science, unless the published structure of
171 vineomycin C requires revision. Possible annotations are reported in Fig. 3. These alternative
172 proposals could account for the preferential fragmentation observed in the MS² spectrum. The
173 proximity of **7a** with fridamycin D (**6a**) in the MN suggested that the most probable annotation
174 might be the one in which aculose underwent a Michael addition, as in **6a**.

175



177

177 **Figure 3.** Published structure of vineomycin C and putative structures for compound **6a**. The
178 sugar groups annotated as rhodinose are either rhodinose or amicetose (indistinguishable
179 stereoisomers in MS).

180 A minor isomer of **7b** also appeared in the MN under the same cluster. Based on the same
181 considerations as for **7a**, **7b** could not be annotated as vineomycin C either. It was therefore
182 new to Science. Next to both **6** and **7**, compound **8** protonated molecular ions at m/z 545.1808
183 corresponded to the formula C₃₁H₂₉O₉⁺ (Calcd. 545.1806). The formula suggested that **8** might
184 be marangucycline B³⁷. Sirius also annotated this compound as marangucycline B, although
185 with 58% confidence only. Marangucycline B is an analog of fridamycin D with a modified
186 aglycone. The presence of an aculose subunit has been confirmed by MS² (m/z 111.0442), but

187 the fragmentation pattern was not attributable to marangucycline B. Hence, while this
188 compound is probably not marangucycline B it could not be annotated further. Angucycline **9**
189 was also new to Science. Its protonated molecular ion at m/z 667.2753 corresponded to the
190 formula $C_{36}H_{43}O_{12}^+$ (Calcd. 667.2749). In the MS^2 spectrum, the fragmentation from the
191 protonated molecular ion to product at m/z 579.1851 corresponded to the loss of a neutral
192 fragment the formula of which was $C_5H_{12}O$ (Fig. S22, Supporting Information). This group has
193 been annotated above as an isopentanol, probably linked to the carboxylic acid moiety. A
194 carbon monoxide loss was also detected from m/z 561.1750 to 533.1812, indicating that the
195 carboxylic acid side chain of the aglycone should be present. The MS^2 spectrum also showed a
196 hydrated aculose oxonium ion at m/z 129.0549 and its dehydrated form at m/z 111.0443. For all
197 these reasons, compound **9** was annotated as shown in Table 1. The protonated molecular ion
198 of compound **10** was found at m/z 781.3438, a mass that corresponds to the formula $C_{42}H_{53}O_{14}^+$
199 (Calcd. 781.3430). An isopentanol, a rhodiose/amicetose, and an aculose were pointed out in
200 the fragmentation spectrum of the parent ion. Rhodiose and aculose oxonium ions were also
201 detected at m/z 115.0754 and 111.0442, respectively, showing that **10** should be annotated as
202 the isopentanol ester of **7a/b**. The formula of compound **11a** protonated molecular ion was
203 found to be $C_{42}H_{53}O_{14}^+$ (exp. m/z 675.2438, calcd. 675.2436). This corresponded to the
204 grincamycin H molecular formula³⁸. Nonetheless, the MS^2 spectrum indicated that **11a**
205 successively lost rhodiose/amicetose and aculose, and therefore could not be annotated as
206 grincamycin H. The mass of the protonated aglycone after oses fragmentation was m/z
207 451.1388, corresponding to a doubly dehydrated fridamycin A. We hypothesized that one
208 hydroxyl group of the olivose side chain might be dehydrated, and that the second H_2O loss
209 might be explained by a ring closing of the lactone as in urdamycin L³⁹, a possibility supported
210 by the analysis of the biosynthetic gene cluster discussed below. Compound **11b** was
211 presumably a minor diastereoisomer of **11a** due to the high similarity of their respective MS^2
212 spectra. Compound **12** protonated molecular ion at m/z 677.2597 indicated the formula
213 $C_{37}H_{41}O_{12}^+$ (Calcd. 677.2593). The MS^2 fragmentation pattern showed the successive losses of
214 rhodiose/amicetose, and aculose. The masses of the fragments generated by cleavage of the
215 aglycone were all shifted by 2 Da relative to those of compound **11a**, indicating that the two
216 additional hydrogens were in the center of the aglycone. Thus, it could be deduced that **12** was
217 likely the hydroquinone form of **11a**. Compound **13** is a minor metabolite and could not be
218 annotated with reasonable confidence. The molecular formula of compound **14** was $C_{49}H_{56}O_{17}$
219 (exp. m/z 917.3601 ($[M+H]^+$), calcd. 917.3590). The MS^2 spectrum indicated a loss of an
220 aculosyl-rhodiose (or aculosyl-amicetose) moiety. Then the product at m/z 675.2443 lost the

221 neutral group C₆H₈O (a dehydro-rhodinose), indicating that the aculosyl-rhodinose moiety was
222 linked to another rhodinose. Then the aglycone ion at m/z 451.1398 was produced by the loss
223 of another aculose. The molecular weight of this aglycone ion (fridamycin A -2 H₂O) along
224 with the proximity of other lactonic aglycones in the MN spoke in favor of **14** also being a
225 lactone derivative, as reported in Table 1. The fragmentation spectrum of compound **15** was not
226 very clear and **15** could not be annotated with enough confidence. At m/z 901.3653, compound
227 **16** protonated molecular ion indicated the formula C₄₉H₅₇O₁₆⁺ (calcd. 901.3641). In MS², the
228 ion **16**+H⁺ lost an aculosyl-rhodinose group to give the product at m/z 659.2499, which then
229 lost dehydro-rhodinose. Further dehydration produced an ion at m/z 545.1790 which again lost
230 aculose to yield the aglycone ion at m/z 435.1471. This aglycone was doubly dehydrated
231 compared to fridamycin A, indicating that the C-oliviosyl group in **16** may be dehydrated. The
232 structure proposed in Table 1 appeared to be a reasonable hypothesis for **16**. The molecular
233 formula of compound **17** is C₄₉H₅₈O₁₈ (exp. m/z 952.3960 ([M+NH₄]⁺), calcd. 952.3961). This
234 molecular formula and sodium adduct fragmentation pattern in which two successive aculosyl-
235 rhodinose losses were recorded were compatible with the annotation of **17** as vineomycin B⁴⁰.

236 In the third part of the fridamycin MN, compounds **18a** and **18b** were annotated as isomers with
237 the molecular formula C₃₁H₃₄O₁₂ (exp. m/z 599.2124 for [M+H]⁺, calcd. 599.2123). Both
238 isomers fragmented extensively in the ESI source to produce the fridamycin A protonated
239 molecular ion [1+H]⁺ losing C₆H₈O₂, *i.e.*, a dehydro-cinerulose A moiety. The cinerulose A
240 oxonium ion was also detected in MS², while the aglycone fragmentation was very similar to
241 what was recorded for [1+H]⁺. Angucyclins **18a** and **18b** were therefore annotated as
242 cinerulosyl-fridamycin A or B. The position of the cinerulosyl side chain was not determined
243 and may not be identical for both isomers. Compounds **19a** and **19b** were annotated as isomers
244 with the molecular formula C₃₁H₃₆O₁₂ (exp. m/z 601.2284 for [M+H]⁺, calcd. 601.2279). Both
245 isomers also fragmented extensively in the ESI source to produce the fridamycin A protonated
246 molecular ion [1+H]⁺ losing C₆H₁₀O₂, *i.e.*, dehydro-rhodinose/amicetose subunit, the
247 corresponding oxonium of which was also present in MS². As mentioned above, the MS²
248 spectrum of the aglycone protonated ion formed by in-source fragmentation was identical to
249 the one of [1+H]⁺, therefore confirming that **19a** or **b** should not be annotated as grincamycin
250 L⁴¹. Instead, **19a** and **19b** were annotated as rhodinოსyl- and/or amicetosyl-fridamycin A/B and
251 should be considered as new to Science. Angucycline **19a** was one of the major constituents in
252 the profile of the strain. Compound **20** molecular formula was C₃₁H₃₄O₁₁ (exp. m/z 583.2170
253 for [M+H]⁺, calcd. 583.2174). Its MS² spectrum showed a rhodinose/amicetose subunit and a

254 dehydrated protonated aglycone. Therefore, compound **20** was annotated as a dehydro-**19a**.
255 Compound **21** molecular formula was $C_{37}H_{45}O_{13}$ (exp. m/z 697.2861 for $[M+H]^+$, calcd.
256 697.2855). Its MS^2 spectrum revealed the successive loss of two rhodinose/amicetose subunits,
257 yielding a dehydrated protonated aglycone. It was thus annotated as shown in Table 1.
258 Compound **22** molecular formula was $C_{31}H_{37}O_{11}$ (exp. m/z 585.2333 for $[M+H]^+$, calcd.
259 585.2330). Its MS^2 spectrum showed the loss of one rhodinose/amicetose subunit, yielding a
260 protonated deoxy-aglycone. The structure of the aglycone could not be readily inferred from
261 the MS^2 spectrum and compound **22** could not be annotated further. Compound **23**'s molecular
262 formula was $C_{37}H_{44}O_{14}$ (exp. m/z 713.2782 for $[M+H]^+$, calcd. 713.2804). A
263 rhodinose/amicetose was visible in MS, but the MS^2 spectrum was impure and further
264 annotation was not possible. Compound **24** molecular formula was $C_{34}H_{41}NO_{13}$ (exp. m/z
265 672.2655 for $[M+H]^+$, calcd. 672.2652). Its MS^2 spectrum showed the loss of 1
266 rhodinose/amicetose subunit yielding a product at m/z 558.1983 ($C_{28}H_{32}NO_{11}^+$), which then
267 successively lost water, CH_2O_2 (formic acid or H_2O+CO), and C_2H_5N to generate a protonated
268 didehydro-fridamycin A at m/z 451.1393. This fragmentation pattern was compatible with **24**
269 being an alanine amide of **19**, as shown in Table 1. The presence of an alanine subunit was also
270 supported by the fragment ion at m/z 90.0550, corresponding to an alaninium ion⁴². Compound
271 **25** molecular formula was $C_{37}H_{46}N_2O_{14}$ (exp. m/z 743.3026 for $[M+H]^+$, calcd. 743.3022). In-
272 source fragmentation indicated the successive loss of a dehydro-rhodinose/amicetose group and
273 a $C_6H_{10}N_2O_2$ subunit. The MS^2 spectrum highlighted the loss of one dehydro-
274 rhodinose/amicetose and two alanine subunits to generate the protonated didehydro-fridamycin
275 A at m/z 451.1393 (see Fig. S64, Supporting information). Overall, compound **25** could be
276 annotated with high confidence as shown in Table 1. Neighboring minor compound **26** in the
277 MN could not be annotate. Compound **27** was an analog of **25** with one rhodinose/amicetose
278 subunit more, the presence of which could be ascertained by examination of both in-source
279 fragmentation scheme and the collision-induced MS^2 spectrum. Compound **28** molecular
280 formula was $C_{37}H_{40}O_{14}$ (exp. m/z 709.2490 for $[M+H]^+$, calcd. 709.2491). The MS^2 spectrum
281 clearly indicated that the protonated molecular ion lost both dehydro-rhodinose/amicetose and
282 a $C_6H_8O_4$ neutral fragment, therefore confirming that this compound was new and should not
283 be annotated as saprolmycin B⁴³. However, the annotation remained ambiguous and **28** was not
284 annotated further. Compounds **29** and **30** were analogs of **28**; **29** did not have the
285 rhodinose/amicetose subunit, while **30** had an aculose in place of the rhodinose/amicetose. All
286 the annotated compounds' MS^2 spectra were provided in the supporting information (Figs S1-

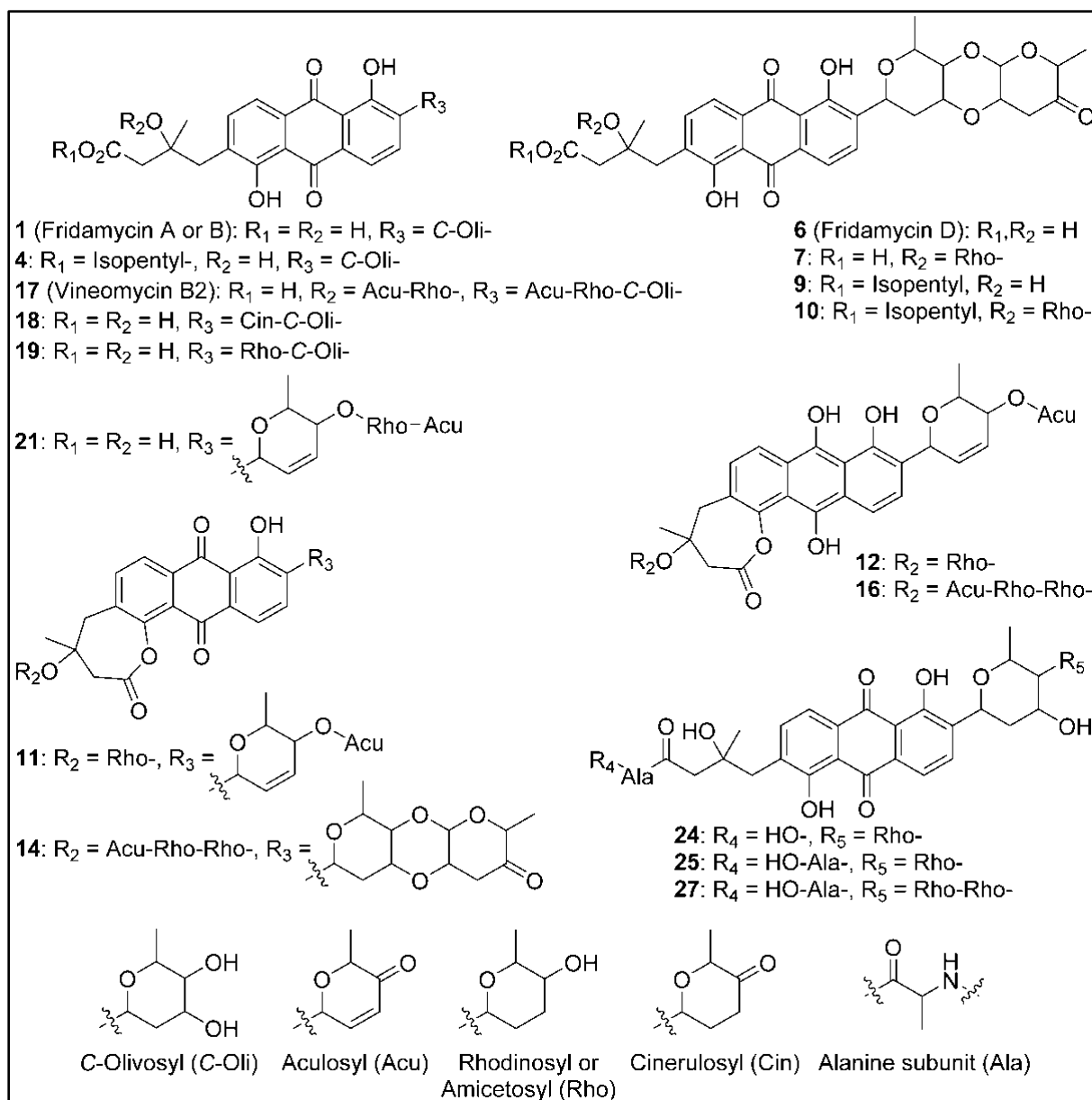
287 [S74](#), Supporting Information), and a list of sugars potentially linked to the angucyclins is
 288 provided in Table [S1](#).

289 **Table 1.** Annotated angucyclines in the metabolomic profile of strain RO-S4

	<i>m/z</i>	Ion type	Molecular formula	$\#$	<i>t_R</i> (min)	Annotation ^b
1	487.1600	[M+H] ⁺	C ₂₅ H ₂₆ O ₁₀	1	8.59	Fridamycin A or B (Fig. 4)
2^c	469.1492	[M+H] ⁺	C ₂₅ H ₂₄ O ₉	1	8.48	[1-H ₂ O]
3^c	529.1708	[M+H] ⁺	C ₂₇ H ₂₉ O ₁₁	1	8.58	Acetyl-fridamycin A or B
4^c	557.2383	[M+H] ⁺	C ₃₀ H ₃₆ O ₁₀	1	11.69	See Fig. 4
5^c	669.2903	[M+H] ⁺	C ₃₆ H ₄₄ O ₁₂	1	13.08	n.a.
6	a: 597.1973	[M+H] ⁺	C ₃₁ H ₃₂ O ₁₂	2	a: 11.01	a: Fridamycin D (Fig. 4)
	b: 597.1969				b: 12.57	
7^c	a: 711.2650	[M+H] ⁺	C ₃₇ H ₄₂ O ₁₄	2	a: 11.87	See Fig. 4
	b: 711.2656				b: 11.17	
8^c	545.1808	[M+H] ⁺	C ₃₁ H ₂₈ O ₉	1	14.21	n.a.
9^c	667.2751	[M+H] ⁺	C ₄₆ H ₄₂ O ₁₂	1	13.66	See Fig. 4
10^c	781.3436	[M+H] ⁺	C ₄₂ H ₅₂ O ₁₄	1	14.31	See Fig. 4
11^c	a: 675.2438	[M+H] ⁺	C ₃₇ H ₃₈ O ₁₂	2	a: 13.74	See Fig. 4
	b: 675.2436				b: 13.10	
12^c	677.2597	[M+H] ⁺	C ₃₇ H ₄₀ O ₁₂	1	11.02	See Fig. 4
13^c	763.3328	[M+H] ⁺	C ₄₂ H ₅₀ O ₁₃	1	12.88	n.a.
14^c	917.3601	[M+H] ⁺	C ₄₉ H ₅₆ O ₁₇	1	12.03	See Fig. 4
15^c	a: 819.2863	[M+H] ⁺	C ₄₃ H ₄₆ O ₁₆	2	a: 12.64	n.a.
	b: 819.2869				b: 12.95	
16^c	901.3647	[M+H] ⁺	C ₄₉ H ₅₆ O ₁₆	1	12.94	See Fig. 4
17	952.3957	[M+NH ₄] ⁺	C ₄₉ H ₅₈ O ₁₈	1	12.27	Vineomycin B2 (Fig. 4)
18^c	a: 599.2124	[M+H] ⁺	C ₃₁ H ₃₄ O ₁₂	2	a: 10.11	See Fig. 4
	b: 599.2125				b: 10.53	
19^c	a: 601.2284	[M+H] ⁺	C ₃₁ H ₃₆ O ₁₂	2	a: 10.06	See Fig. 4
	b: 601.2288				b: 10.95	

20^c	583.2170	[M+H] ⁺	C ₃₁ H ₃₄ O ₁₁	1	8.62	[19a -H ₂ O]
21^c	697.2861	[M+H] ⁺	C ₃₇ H ₄₄ O ₁₃	1	9.32	See Fig. 4
22^c	585.2333	[M+H] ⁺	C ₃₁ H ₃₆ O ₁₁	1	10.87	n.a.
23	713.2782	[M+H] ⁺	C ₃₇ H ₄₄ O ₁₄	1	11.88	n.a.
24^c	672.2655	[M+H] ⁺	C ₃₄ H ₄₁ NO ₁₃	1	9.70	See Fig. 4
25^c	743.3031	[M+H] ⁺	C ₃₇ H ₄₆ N ₂ O ₁₄	1	9.44	See Fig. 4
26^c	813.3816	[M+H] ⁺	C ₄₂ H ₅₆ N ₂ O ₁₄	1	11.55	n.a.
27^c	857.3709	[M+H] ⁺	C ₄₂ H ₅₆ N ₂ O ₁₄	1	10.24	See Fig. 4
28^c	709.2490	[M+H] ⁺	C ₃₇ H ₄₀ O ₁₄	1	10.95	n.a.
29^c	595.1808	[M+H] ⁺	C ₃₁ H ₃₀ O ₁₂	1	9.47	n.a.
30^c	705.2182	[M+H] ⁺	C ₃₇ H ₃₆ O ₁₄	1	11.83	n.a.

290 ^aNumber of isomers detected in the MN cluster. ^bProposed structures are annotations based on
291 literature data and automatic and manual analysis of MS² spectra. n.a.: not annotated. ^cNovel
292 compound.



293

294 **Figure 4.** Annotated metabolites from Strain RO-S4. Stereocenters are intentionally drawn as
 295 undefined. Only the raw formula of the substituents can be inferred from the mass spectra. Their
 296 developed formulas and relative positions are putative.

297 Whole genome sequencing

298 The whole genome of *Streptomyces* sp. RO-S4 was sequenced using the Illumina Novaseq
 299 technology. The complete genome consisted of 7,497,846 bp with 72.4% G+C content. The
 300 closest genome to *Streptomyces* sp. RO-S4 sequenced from a type strain was that of *S.*
 301 *althoticus* JCM 4344 (assembly GCA_014649355; 90.73% ANI), and that of *S. tendae* strain
 302 139 (CP04395; 95.84%) for a non-type strain. The genome of *Streptomyces albogriseolus*

303 NRRL B-1305, the closest strain based on 16S rRNA gene similarity was not available at the
304 time of analysis.

305 **Secondary metabolite biosynthetic gene clusters of *Streptomyces* sp. RO-S4**

306 The genome of the RO-S4 strain was analyzed by the antibiotics & Secondary Metabolite shell
307 (antiSMASH) to determine its putative biosynthetic capabilities. A total of 19 putative
308 biosynthetic gene clusters were annotated (Table S2, supporting information), including three
309 types of polyketide synthases BGCs [Type 1 (T1PKS), Type 2 (T2PKS), and type 2 (T3PKS)]
310 polyketide synthases, class I Lanthipeptides, a Lasso peptide, a Ribosomally Synthesized and
311 Post-Translationally Modified Peptide (RiPP), an Ectoine, a Terpene, Phenazines, and a
312 Butyrolactone BGC. In addition, four hybrid clusters were recovered that were composed of 1)
313 T2PKS, Oligosaccharide Phenazine, Siderophore, 2) RiPP-like, betalactam, Terpene, 3) Two
314 hybrid Non-ribosomal Peptide Synthase (NRPS), and T1PKS. The analysis showed that 17 out
315 of the 19 identified BGCs showed high content similarity with known BGCs, five of which (3,
316 5, 7, 13, and 17) showed 100% content similarity with known BGCs. Two clusters (Cluster 10
317 and 16) were annotated as orphan BGCs for which no homologous gene clusters could be
318 identified, suggesting that they could be responsible for the biosynthesis of novel natural
319 products or natural products with no characterized BGCs. Many of these clusters are known to
320 encode genes linked to the production of biologically active natural compounds, such as
321 antibiotics. Notably, we have recovered a T2PKS BGC very similar to those linked to the
322 biosynthesis of angucycline compounds, consistent with the metabolomic analysis.

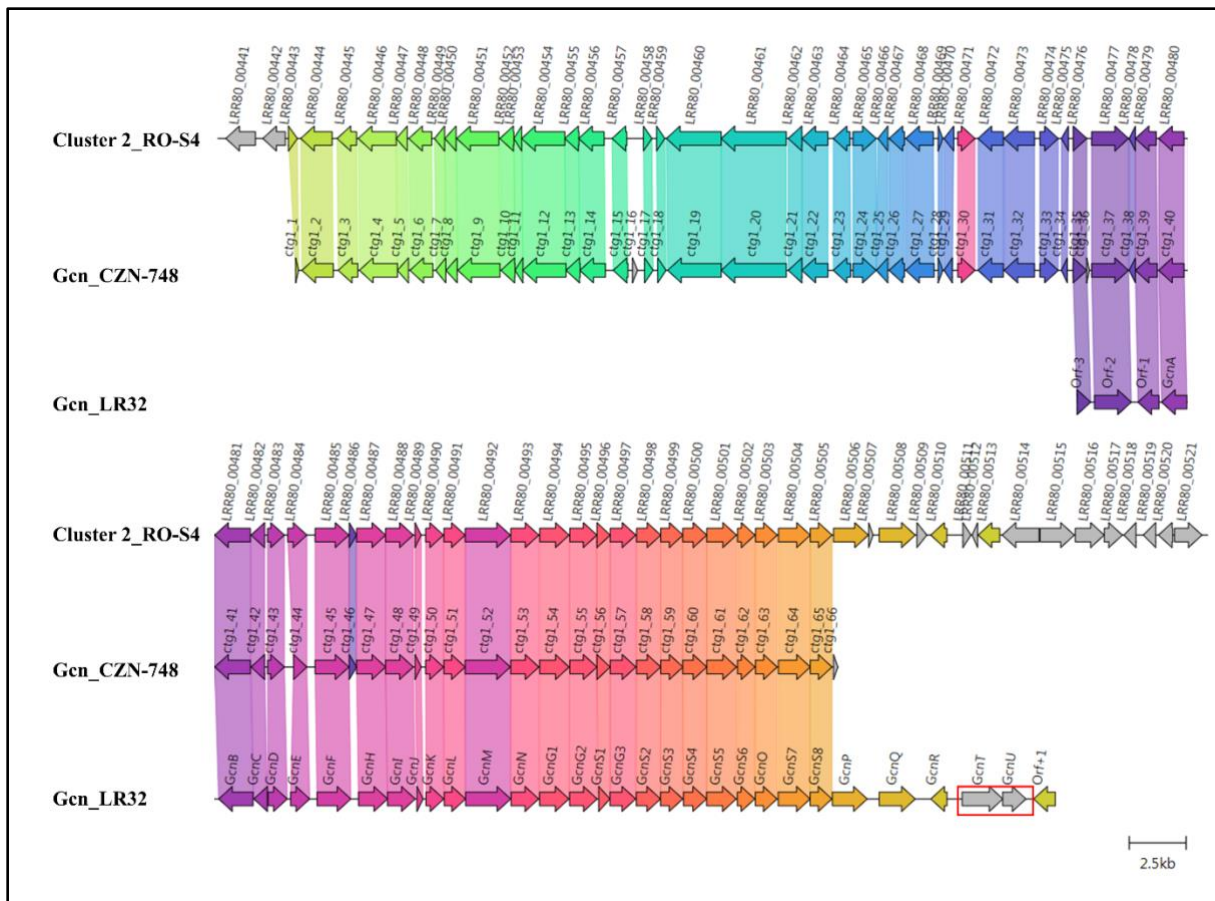
323 **Description of the Angucycline Biosynthetic Gene Cluster**

324 AntiSMASH analysis using an unannotated genomic DNA sequence revealed that Cluster 2 in
325 Contig ROS4_2 of the assembly displayed a high synteny (> 65% common genes) to that of
326 BGCs linked to several angucycline compounds, such as grincamycin (97%), saprolmycin E
327 (83%), saquayamycin A (75%), landomycin A (71%), and saquayamycin Z (67%). All these
328 compounds share a common tetracyclic angular benz[a]anthraquinone aglycone. Due to the
329 predominance of tricyclic aglycones ("open" aglycone(s) hereafter) among the major
330 metabolites of RO-S4, we performed an in-depth analysis of Cluster 2.

331 Cluster 2 contains genes putatively involved in the biosynthesis and modification of the
332 aglycone core. A typical set of genes responsible for an angucycline core assembly named
333 "minimal PKS" has been identified supporting the synthesis of angucycline like molecules by
334 his cluster. This included three genes: a ketoacyl synthase α (LRR80_00487), a ketoacyl
335 synthase β /chain length factor CLF (LRR80_00488) and an acyl carrier protein (ACP)

336 (LRR80_004989). Two possible cyclase genes (LRR80_00486 and LRR80_00491) were also
337 annotated, which are likely responsible for the polyketide chain cyclization into the
338 benz[a]anthracene structure. In addition, this cluster harbors two genes encoding oxygenase
339 enzymes (LRR80_00485 and LRR80_00492) probably involved in the modification of the
340 aglycone and possibly in the lactonization and opening of the angular aglycone cycle (see
341 discussion below). (Keto)reductase-coding genes, including LRR80_00490 and
342 LRR80_00470, were annotated to exhibit a high degree of sequence similarity to known
343 enzymes involved in the modification of aromatic polyketides. Three genes (LRR80_00495,
344 LRR80_00496, and LRR80_00498) likely associated with the glycosylation steps showed high
345 similarity to genes coding glycosyltransferases (GTs) in other angucyclines. All the annotated
346 genes involved in the BGC of Cluster 2 and their homologs are listed in Table S3.

347 The closest BGCs to RO-S4 Cluster-2 are those of the grincamycin-producing *Streptomyces*
348 *lusitanus* SCSIO LR32 (Gcn LR32)⁴⁴, and *Streptomyces* sp. CZN-748 (Gcn CZN-748)³⁴
349 graciously provided by the authors). We performed a synteny analysis comparing the three
350 BGCs and notably, when PROKKA⁴⁵-annotations were used for RO-S4 and CZN-748, the
351 *gcnM* ORF was absent in these strains, as previously described by Shang and co-workers³⁴. In
352 contrast, the BGC annotated by AntiSMASH from genomic sequences identified these ORFs.
353 This difference could be explained by a possible tRNA_{ala} in the region coding the *gcnM*
354 orthologs (Fig. S75, Supporting Information). In addition, the comparison between the BGC of
355 LR32 identified two missing genes (*gcnU* and *gcnT*) in the BGC of ROS4_2, whereas the region
356 downstream of *gcnS8* was not present in the available BGC of strain CZN-748 (Fig. 5). Cluster
357 2 of RO-S4 showed near complete synteny and a higher average amino acid identity (99.8 %
358 for 28 common ORFs) to the grincamycin BGC of CZN-748, which fits the observation that
359 both strains produce a majority of "open" aglycone angucyclines, whereas LR32 (93.2 %
360 average amino acid identity for 28 common ORFs) produces primarily tetracyclic angucyclines,
361 as previously noted by Shang and co-workers³⁴.



362
 363 **Figure 5.** Comparison between Cluster 2 of *Streptomyces* sp. RO-S4, the Grincamycin Gene
 364 Cluster of *Streptomyces lusitanus* SCSIO LR32, and the BGC of Grincamycin-producing
 365 *Streptomyces* sp. CNZ-748. Gene neighborhoods representative of the compared BGCs are
 366 shown aligned with an arbitrary color scheme using clinker to highlight the conserved genes.
 367 Missing genes in RO-S4 compared to LR-32 were highlighted in red.

368 Discussion

369 Here we report the use of a combined genomic-metabolomic approach to investigate the
 370 antagonistic potential of the *Streptomyces* sp. RO-S4 strain isolated from a polluted marine
 371 environment. Based on 16S rRNA gene sequencing and genomic analysis, the strain belongs to
 372 the genus *Streptomyces*, but it was not possible to assign it to a species. RO-S4 extracts show
 373 inhibitory activity against MRSA with a MIC of 16 µg/mL.

374 Metabolomic analyses of the crude extract produced by the RO-S4 strain using mass-
 375 spectrometry-based molecular networking revealed diverse angucycline derivatives as
 376 dominant products, which have mostly (but not exclusively) been linked to the *Streptomyces*
 377 genus^{46,47}. Angucyclines represent the largest group of type 2 PKS natural products produced
 378 by actinobacteria, and they show diverse pharmacological activities including cytotoxicity,
 379 antitumor, antibacterial, and antiviral properties^{48,49}.

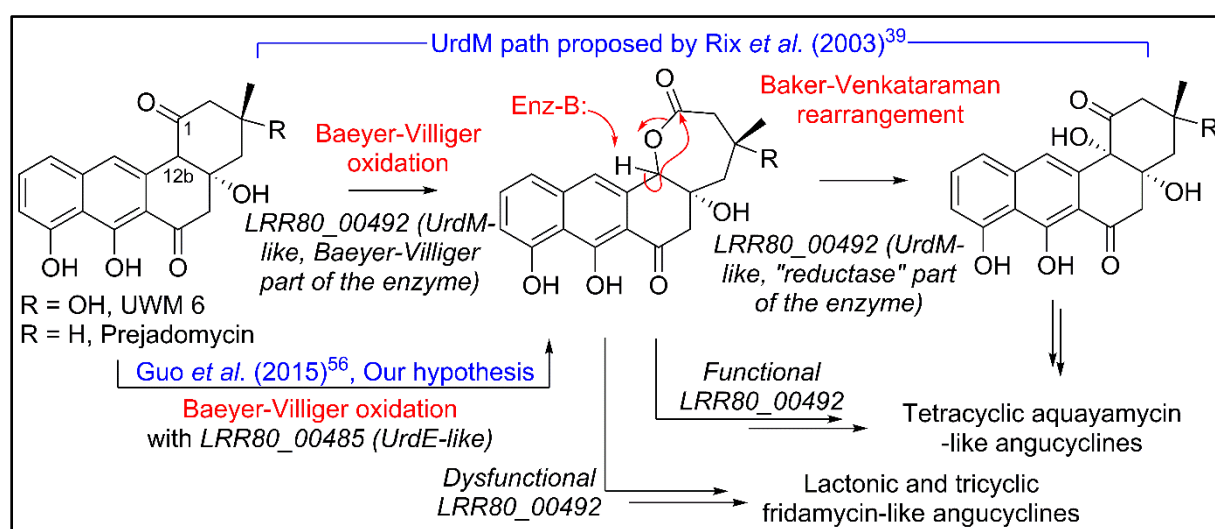
380 We have demonstrated that many of the compounds identified by our untargeted metabolomic
381 analysis are novel to Science, and this high diversity of novel molecules can be explained by
382 the ability of HRMS to highlight minor compounds even though some of the major metabolites
383 are also new to Science. Our annotation of the RO-S4 angucycline-like compounds was further
384 supported by genomic analysis.

385 The combination of metabolomic and genome analysis provides some interesting insights into
386 the biosynthesis of angucyclines. Cluster 2 shows high content, synteny, and sequence
387 similarity to previously described BGCs of grincamycin-like products and is certainly
388 responsible for producing the structures predicted by the MN analysis. Since the RO-S4 strain
389 and *Streptomyces* CNZ-748 produce primarily tricyclic glycosylated structures, while LR32
390 and many other strains produce tetracyclic angucyclines, we were interested in possible
391 enzymatic processes that could lead to the biosynthesis of these tricyclic aglycons³⁴. Several
392 studies have indicated that oxygenase complexes are required for cyclic C-C bond cleavage, in
393 particular Baeyer-Villiger type oxygenases⁵⁰. In the case of RO-S4 products, we hypothesized
394 that this reaction would take place by an oxidation of the C12b–C1 single bond of the aglycone
395 (an UWM6-like molecule), prior or after glycosylation, and a subsequent hydrolysis of the
396 lactone (Figure 6). We have therefore focused the analysis on putative Baeyer-Villiger mono-
397 oxidases (BVMOs) in Cluster 2 of the RO-S4 strain.

398 The observation that – as in the case of the grincamycin BGC of strain CZN-748 – annotation
399 with PROKKA⁴⁵ failed to identify an ORF downstream of the T2PKS synthases and the cyclase
400 putatively involved in the generation of the angular cycle (the region coding for GcnM in *S.*
401 *lusitanus* LR32⁴⁴), suggested that this ORF could be involved in the ring opening process. Since
402 AntiSMASH identified an ORF both in RO-S4 (LRR80_00492) and CNZ-748 (CTG1-52)
403 when a genomic sequence was used as the query, we determined that PROKKA failed to
404 annotate the ORF since its Aragorn⁵¹ step identified a putative tRNA_{ala} (Fig. S75, Supporting
405 Information) in its complementary strand. However, the facts that the putative tRNA is in the
406 reverse strand, that it contains mismatches in the side harpins, and that 4 more canonical
407 tRNA_{ala} are coded in the genome, suggest that this tRNA_{ala} could have been misidentified. We
408 performed an RNA fold analysis⁵² that identified a highly probable and low-entropy hairpin
409 loop that could potentially affect the translation of this ORF (Fig. S76, Supporting Information)
410 and possibly decreases the production of the coded protein.

411 The LRR80_00492 ORF codes a hybrid FAD-dependent oxidase-reductase (GcnM in the
412 grincamycin BGC) homologous to UrdM, that has been linked to C12b hydroxylation in the

413 biosynthesis of urdamycins by *S. fradiae* TÛ 2717^{53,39}. Furthermore, a mutant with an in-frame
 414 deletion of the reductase domain of UrdM produced small amounts of urdamycin-L, a product
 415 containing an oxygen between C12b and C1, leading to the hypothesis that UrdM is involved
 416 in the C12b–C1 bond oxidation and subsequent lactone Baker-Venkataraman rearrangement
 417 leading to the tetracyclic skeleton of aquayamycin-like angucyclins (Fig. 6)³⁹. However, in this
 418 model, low levels, or absence of LRR80_00492 due to the secondary structure described above
 419 would not lead to fridamycin-like aglycones as those in RO-S4 (Table 1), and another BVMO
 420 should be responsible for the oxidation of the C12b–C1 bond in **UWM 6** (or other
 421 intermediates) leading to compounds **11**, **12** and, **16** and fridamycin-like aglycones.



422

423 **Figure 6.** Hypotheses for conversion of UWM 6 or prejadomycin into angucyclines.

424 The BGC of RO-S4 and of all grincamycin-producing strains contains a second FAD-dependent
 425 putative BVMO product of LRR80_00485 (GcnE in the grincamycin BGC) that is homologous
 426 to FAD-dependent monooxygenases involved in angucycline modifications (e.g. UrdE, PgaE,
 427 BexE, CabE; Fig S77 and S78, Supporting Information). In earlier studies, UrdE was
 428 hypothesized to directly hydroxylate different positions of the aglycon (C6, C12, C12b)^{53,54,55}
 429 in urdamycin biosynthesis, but more recent evidence have suggested that its homologue PgaE
 430 might also oxidize the C12b–C1 bond of prejadomycin leading to the tricyclic aglycons of
 431 gaudimycins D and E⁵⁶. *In vitro* assays using enzymes heterologous expressed in *E. coli* also
 432 showed that PgaE/CabE oxidizes UWM6 and is dependent on the PgaM_{red} homologue CabV to
 433 complete the hydroxylation of UWM6 at C12b⁵⁷.

434 Since in the RO-S4 BGC there are two possible FAD-dependent mono-oxidases that could be
 435 involved in oxidation of the C12b–C1 bond and subsequent ring opening of RO-S4 and CNZ-

436 748, we attempted to compare the sequences of both ORFs to different enzymes oxidizing
437 analogous cyclic compounds, including MtmOIV, shown to perform a Baeyer-Villiger
438 oxidation and ring opening of premithramycin B to mithramycin. *Blastp* analyses indicated that
439 the LRR80_00492 (UrdM like)/mtmOIV alignment was shorter and had a lower overall score,
440 but a higher number of identical positions, whereas the LRR80_00485 (UrdE-like)/mtmOIV
441 alignment was longer and had a higher total score, but with fewer identical positions.
442 Phylogenetic analyses including UrdE homologues and the oxidase portion of UrdM
443 homologues separated these oxidases into two groups, with maximum likelihood and distance
444 methods showing that LRR80_00485 was slightly closer to MtmOIV than LRR80_00492, and
445 in a subclade including PgaE (Figs. [S77](#) and [S78](#), Supporting Information).

446 In aggregate, these results lead to different possibilities that could be tested in the future using
447 genetic modifications of the different ORFs in the angucyline BGC of the RO-S4 strain or
448 CNZ-748. Hypothesis 1): the product of LRR80_00492 would be solely responsible for
449 oxidation of the C12b–C1 bond. This hypothesis is supported by the prediction that this enzyme
450 has several AAs unique to RO-S4 and CNZ-748. On the other hand, since the reductase portion
451 of the enzyme is present, one would expect that tetracyclic angucyclines with a hydroxylated
452 C12b would be produced. Hypothesis 2): the most likely hypothesis based on our work on the
453 RO-S4 strain is that the LRR80_00492 ORF is inactive due to the presence of a tRNA_{ala} in the
454 coding region or that its translation is affected by secondary structure, in which case
455 LRR80_00485 would generate the lactone via a Baeyer-Villiger oxidation, possibly allowing
456 for a later opening of the ring. Other alternative hypotheses that could be related to the ring
457 opening are: Hypothesis 3): that the LRR80_00492 ORF would be partly transcribed due to the
458 mRNA secondary structure, which would allow its oxidase portion to be transcribed but not the
459 reductase, much like the case with the *urdM* partial knockout mutant that produces urdamycin
460 L³⁹ and is responsible for C12b–C1 single bond oxidation, and Hypothesis 4): another BVMO
461 enzyme not in the BGC could be responsible for ring opening. The genome of RO-S4 codes for
462 another enzyme with a slightly higher *blastp* score when queried with MtmOIV. That ORF is
463 present in a hybrid NRPS-T1PKS hybrid BGC similar to that of polyoxypeptin A BGC⁵⁸.
464 However, the function of that homologue (ORF4) in the polyoxypeptin A BGC has not yet been
465 described.

466 In addition to these oxygenases, three genes are presumed to code for glycosyltransferase (GT)
467 enzymes, which show similarities to known GTs involved in angucycline biosynthesis. The
468 first, RO-LRR80_00495, shows high homology to GcnG1 (96.98%⁴⁴), sqnG1 (88.14%⁵⁹),

469 sprGT1 (86.74%⁶⁰), and SchS10 (81.63%⁶¹). The second (LRR80_00496) is closely related to
470 GcnG2 (92.46%⁴⁴), sprGT2 (83.92%⁶⁰), sqnG2 (81.91%⁵⁹), and schS9 (74.74%⁶¹). The third
471 GT (LRR80_00498) is most similar to enzymes involved in the glycosylation of D-olivose at
472 the C9 position of several angucycline-like molecules [ex. SchS7 in the Sch-47554 biosynthetic
473 gene cluster⁶¹; SprGT3 in saprolmycin biosynthesis⁶⁰; UrdGT2 in urdamycin biosynthesis in
474 *Streptomyces fradiae* Tü 2717⁶², among others], supporting well the predicted structures in
475 Table 1, all of which are predicted to have been glycosylated with an olivose at the C9-position.
476 SchS9 and SchS10 are thought to be *O*-glycosyltransferases involved in the biosynthesis of
477 Sch-47554⁶¹. Genetic studies using heterologous expression and targeted gene disruption have
478 shown that SchS7 attaches D-amicetose at C-9 and SchS9 further extends the saccharide chain,
479 while SchS10 attaches L-aculose at the C-3 position⁶³. The SqnGT1-G3 are glycotransferases
480 involved in the biosynthesis of saquayamycin A in *Streptomyces sp.* KY40-1. According to
481 genetic experimentation, sqnG2 was identified as catalyzing both *O*- and *C*-glycosylations⁵⁹.

482 Hence, based on similarities between known GTs and the sugars annotated by metabolomic
483 analysis, we hypothesize that a D-olivose is added to C9 by LRR80_00498 and further *O*-
484 glycosylated with rhodinose/amicetose by one of the three glycosylases, and in some cases (ex.
485 compound **9**), experiencing a Michael addition, or further glycosylation as in compounds **19**
486 and **27** (and in previously described angucyclines). Interestingly, all compounds glycosylated
487 at position C3 in RO-S4 appear to have a rhodinose/amicetose as the sugar moiety, as do all
488 grincamycins. It is worth noting that the composition and varying lengths of the oligosaccharide
489 chains in angucyclines have a considerable impact on their biological potential, as previously
490 reported by Elshahawi *et al.*⁶⁴.

491 In addition to the rare lactonized D cycle, we also detected other modifications that, to the best
492 of our knowledge, have so far not been shown for fridamycin-like molecules, including alanyl
493 amidation(s) (compounds **25-28**). Amide modifications have been previously shown in
494 fridamycin G⁶⁵, and fridamycin I produced by *Actinokineospora spheciospongiae*⁶⁶.
495 Fridamycin G contains an ethanolamine moiety and was produced heterologously, and the
496 amidation was attributed to a process linked to the host, since the BGC source (*S. cyanogenus*
497 S136) does not produce it. Fridamycin I contains a benzylamine moiety, the biosynthetic origin
498 of which was not discussed. As compounds **25-28** contain multiple alanine moieties, we
499 speculate that fridamycin-like molecules could undergo peptide-like elongation with
500 aminoacids (alanine or *L-p*-hydroxyphenylglycine in the case of fridamycin I), perhaps via an
501 NRPS in a manner analogous to what has been described in the biosynthesis of actinomycin-

502 D⁶⁷. The presence of an *hpgT* homologue – the enzyme linked to L-*p*-hydroxyphenylglycine
503 production in actinobacteria⁶⁸ – in the *Actinokineospora spheciospongiae*, supports this
504 hypothesis.

505 **Conclusions**

506 Our combination of untargeted UPLC-HRMS/MS metabolomic, molecular networking, and
507 genomic analyses generated many structural and biosynthetic hypotheses for targeted structural
508 determination and genetic manipulation, possibly using recently developed gene editing
509 approaches (e.g.^{69,70}). This approach does not substitute traditional isolation-NMR structural
510 analyses and genetic manipulations, which ultimately will be needed to confirm these
511 hypotheses. However, as it yields structural information of many minor compounds linked to
512 BGCs in a relatively fast manner, it can streamline and accelerate pipelines of discovery of new
513 drugs, biosynthetic pathways, and enzymes, and hopefully inspire the discovery to novel
514 antibiotics effective against multi-resistant microorganisms.

515 **Methods**

516 **Isolation of the RO-S4 strain**

517 The RO-S4 strain was isolated from polluted seawater that was collected from the coastline of
518 Bejaia City (36°43'55.2"N5°04'37.9"E), Algeria on August 2017. It was isolated after filtration
519 onto a 0.22 µm pore size membrane filter as described by⁷¹ and laid onto solid M2 medium
520 prepared according to Jensen *et al.*⁷² with small modifications , which consisted of starch (10
521 g), casein bovine milk (1 g), microbiological agar (18 g), and natural 100% of seawater (1 L),
522 and 1 mL (per liter of final medium) of trace salt solution that was prepared according to
523 Shirling and Gottlieb⁷³.

524 **Molecular identification of the RO-S4 isolate**

525 The initial molecular identification of the RO-S4 strain was based on the 16S rRNA gene
526 sequence. Genomic DNA was extracted from the grown strain using the Wizard® Genomic
527 DNA Purification Kit (Promega, USA) according to the manufacturer's instructions. PCR and
528 sequencing were realized as previously described⁷⁴, utilizing universal primers recommended
529 for bacteria 27F mod: 5'AGRGTTTGATCMTGGCTCAG 3' and 1492R mod:
530 5'TACGGYTACCTTGTTAYGACTT 3'. The PCR product was purified with a purification
531 kit (Promega, USA), and then sequenced by the dideoxy termination reaction using an AB3130
532 DNAXl sequencer. The obtained 16S rRNA sequence was identified by comparison to the

533 EZBiocloud database (<https://www.ezbiocloud.net/>) recommended by Yoon and co-workers⁷⁵.
534 The RO-S4 16S rRNA gene sequence was deposited in the GenBank database under the
535 accession number (MW448345)

536 **Antimicrobial Assays**

537 The antibacterial potential of RO-S4 isolate was evaluated against *methicillin-resistant*
538 *Staphylococcus aureus* (MRSA) ATCC 43300 by the agar diffusion method⁷⁶. 8 mm diameter
539 agar cylinders of the RO-S4 strain (M2 medium, incubation for 14 days at 28 °C) were inserted
540 into Muller Hinton plates previously seeded with the targeted bacterium at 10⁷ UFC/mL. The
541 plates were placed for 2 h at 4 °C and antibacterial activity was estimated by measuring the
542 inhibition zone around the agar disc after incubation of the plates for 24 h at 37 °C.

543 **Culture strain and the production of raw extract**

544 The production of bioactive compounds by the selected strain was carried out by agar surface
545 fermentation (ASF), according to Nkanga and Hagedorn⁷⁷. Briefly, the RO-S4 isolate was
546 initially grown on M2 agar plates. After 14 days, the mycelium layers were peeled off and
547 extracted overnight in ethyl acetate (EtOAc), covering the entire surface, and the ethyl acetate
548 extract was drawn. Subsequently, the organic extract was concentrated under vacuum with a
549 rotary evaporator at 40 °C and then stored at -80 °C until further analysis. A control,
550 uninoculated medium, was extracted with the same protocol.

551 **Minimum Inhibitory Concentration (MIC) of the RO-S4 crude extract**

552 The minimal inhibitory concentration (MIC) of the RO-S4 EtOAc extract was evaluated against
553 the MRSA ATCC 43300 strain by the broth microdilution method as recommended by the
554 Clinical and Laboratory Standards Institute⁷⁸. The assays were performed in serial dilutions (in
555 triplicate) in 96-well plates. Briefly, the EtOAc extract was diluted in DMSO and tested at
556 different concentrations ranging from 256 to 0.5 µg/mL. The targeted bacterium culture was
557 prepared in Muller Hinton broth at 2•10⁵ UFC/mL. Afterward, 10 µl of the test bacterial culture
558 was pipetted into each well. The last column (column 12) with no inoculum served as a sterility
559 control, while wells that were not treated with the crude extract served as a negative control
560 (column 11). The final volume of each well was adjusted to 100 µL. The microplate was shaken
561 gently, then incubated for 24 h at 37 °C. Inhibition was evaluated as well, where the growth
562 medium appeared clear, indicating that the test extract prevented the growth or killed the
563 bacteria.

564 **UHPLC-HRMS Profiling**

565 The protocol for high-resolution Full MS data dependent MS² analyses was adapted from
566 previous reports^{79,80}. Here, crude bacterial and culture medium (M2) extracts were dissolved in
567 MeOH at a concentration of 1.5 mg/mL. Pure methanol injections were used as blanks for
568 metabolomics. In HPLC, the solvent system was a mixture of water (solution A) with increasing
569 proportions of acetonitrile (solution B), both solvents modified with 0.1% formic acid. Here,
570 the gradient was as follows: 5% B 5 min before injection, then from 1 to 12 min, a linear
571 increase of B up to 100%, followed by 100% B for 8 min.

572 **MS/MS Molecular Networking analysis and Spectra Annotation**

573 The molecular network was constructed using the Global Natural Product Social networking
574 (GNPS) platform available at: (<https://gnps.ucsd.edu>) as recommended by Wang and
575 collaborators³², using the molecular networking (MN) tool. The MS² data of the crude extract,
576 solvent (blank) and culture media were converted from RAW to mzXML files using the
577 Proteowizard MSConvert tool version (3.0.20104), then uploaded to GNPS. For MN
578 construction, the precursor ion mass tolerance was set at 0.005 Da and the MS² fragment ion
579 tolerance was set at 0.01 Da. A network was created where edges were filtered to have a cosine
580 score above 0.77 and 11 or more matched peaks. The maximum size of a molecular family was
581 set at 85. The MS² spectra in the network were searched against the 'GNPS spectra library'. All
582 matches between network and library spectra were required to have a score above 0.7 and at
583 least 6 matched peaks. Visualization of the molecular network was performed in Cytoscape
584 (3.8.0) which allowed its visualization as a network of nodes and edges⁸¹. Redundancies and
585 adducts were cleared manually. In our Fig. 2, node numbers are consensus parent masses, node
586 size is linked to the relative molecular ion intensity based on peak area measured from the
587 extracted ion chromatogram. Peak areas were measured automatically with the FreeStyle
588 Genesis algorithm, sometimes modified manually if found unfitting, and then pasted manually
589 into the Cytoscape table. This information was also used to create pie charts in which each
590 portion represents the relative peak area of different isomers included in the same node (each
591 GNPS node is a cluster of MS² spectra that may come from different isomeric protonated
592 molecular ions). For nodes gathering protonated molecular ions and in-source fragments of
593 higher molecular weight compounds, only protonated molecular ion integrations were included
594 for peak area information. Any ion present in the network solely due to in-source fragmentation
595 was given the arbitrary extracted ion intensity of 0 and was white in the network. Furthermore,
596 spectra of interest were manually annotated using different databases and tools, including

597 Sirius⁸², Metfrag⁸³ available at (<https://msbi.ipb-halle.de/MetFrag/>), Pubchem, Sci-Finder, and
598 Mass Bank of North America (MoNa, <https://mona.fiehnlab.ucdavis.edu/>). Detailed spectral
599 data are provided in supporting information (Figs. S1-S74, Supporting Information), and the
600 raw spectral files are available (See Data Availability).

601 **Whole Genome Sequencing and Assembly of *Streptomyces* sp. RO-S4 strain**

602 Genomic DNA was isolated from 50 mL of RO-S4 grown in M2 broth medium for 12 days at
603 28 °C with shaking (150 rpm/min). The DNA was extracted using the Bacteria Genomic DNA
604 Extraction Kit (Promega, United States) according to the manufacturer's instructions. Illumina
605 whole genome sequencing was performed by the Genotoul facility in Toulouse, France. Briefly,
606 libraries (Truseq nano HT, Illumina) were constructed using 200 ng of purified DNA and
607 sequenced on a Novaseq 6000 sequencer (Illumina), generating 93 million paired 150 base pair
608 (bp) reads. The entire dataset was assembled using SPAdes (v3.14.0)⁸⁴ with the option
609 "careful". The assembly was manually curated to remove contigs with low (<500) coverage and
610 low (<55%) G+C content. Since a gene cluster of interest was truncated in a contig, we
611 manually extended it using blast searches against raw reads and re-assembly of reads and of a
612 downstream contig using the *gap4* tool of the Staden package (<http://staden.sourceforge.net>).
613 This final assembly was auto-annotated using PROKKA v. 1.14.6⁴⁵ using *Streptomyces* sp.
614 Vc74B-19 protein descriptions and the annotation was manually curated prior to final
615 submission to 1) add the ORF corresponding to GcnM in *Streptomyces* sp. LR32, 2) remove
616 partial rRNA genes and possible adapters in contig ends. The genomic sequence was compared
617 to that of close strains based on the 16S rRNA gene analysis described above, relatives (type
618 strains) and genomes in the NCBI GenBank, based on top *blastp* hits using the five
619 housekeeping genes described by Antony-Babu and coworkers⁸⁵. ANI values were calculated
620 using the OrthoANI tool available through the EZbiocloud server
621 (<https://www.ezbiocloud.net/tools/orthoani>).

622 **Prediction of secondary metabolite biosynthetic gene clusters (BGCs) in the RO-S4** 623 **genome**

624 The sequenced genome (DNA sequence as input) of the RO-S4 strain was analyzed for the
625 prediction of secondary metabolites and biosynthetic gene clusters (BGCs) using the genome
626 mining tool antiSMASH⁸⁶, version 6.0.1. available through
627 (<https://antismash.secondarymetabolites.org>) using the "relaxed" option. Synteny plots of the
628 RO-S4 angucycline BGC was performed using Clinker v 0.0.21⁸⁷. We also submitted the

629 PROKKA annotated genbank formatted files using different annotation parameters. All results
630 as well as descriptions of annotation pipelines are available (see data availability below).

631 **Phylogenetic analysis of UrdE and UrdM homologues**

632 Phylogenetic analysis of UrdE and UrdM homologues in RO-S4 and in the BGCs of other
633 angucyclines and the ring-opening Baeyer-Villiger monooxygenase MtmOIV in the
634 mithramycin BGC was performed using SeaView Version 4.6 and Mega11⁸⁸. Briefly, amino-
635 acid sequences were aligned using muscle and a mask created using the gblocks options "allow
636 smaller blocks positions" and "allow gap positions" followed by manual curation of the mask
637 and a tree were generated by maximum likelihood with the GT+F model and gamma
638 distribution using MEGA11 based on 359 homologous. A neighbor-joining tree was
639 constructed using the JTT substitution model. The robustness of both trees was evaluated by
640 bootstrap analysis using 100 replicates. The raw alignments, the regions used for reconstruction
641 and results of model testing are available (see Data Availability).

642 **References**

- 643 1. Prestinaci, F., Pezzotti, P. & Pantosti, A. Antimicrobial Resistance: A Global Multifaceted
644 Phenomenon. *Pathog Glob Health* **109**, 309–318;
645 <https://doi.org/10.1179/2047773215Y.0000000030> (2015).
- 646 2. Munita, M. & Arias, C.A. Mechanisms of Antibiotic Resistance. Edited by Indira T. Kudva
647 and Qijing Zhang. *Microbiol Spectr* **4**, 1-37; [https://doi.org/10.1128/microbiolspec.VMBF-](https://doi.org/10.1128/microbiolspec.VMBF-0016-2015)
648 [0016-2015](https://doi.org/10.1128/microbiolspec.VMBF-0016-2015) (2016).
- 649 3. Ventola, C.L. The Antibiotic Resistance Crisis. *P & T* **40**, 277-283 (2015).
- 650 4. Chokshi, A., Sifri, Z., Cennimo, D. & Helen Horng. Global Contributors to Antibiotic
651 Resistance. *J Global Infect Dis* **11**, 36-42; https://doi.org/10.4103/jgid.jgid_110_18 (2019).
- 652 5. Chambers, H. F. & DeLeo, F. R. Waves of resistance: *Staphylococcus aureus* in the
653 antibiotic era. *Nat Rev Microbiol* **7**, 629–641 (2009).
- 654 6. Barbosa, F., Pinto, E., Kijjoa, A., Pinto, M. & Sousa, E. Targeting Antimicrobial Drug
655 Resistance with Marine Natural Products. *Int J Antimicrob* **56**, 1-29;
656 <https://doi.org/10.1016/j.ijantimicag.2020.106005> (2020).
- 657 7. Edwards, B et al. Treatment Options for Methicillin-Resistant *Staphylococcus Aureus*
658 (MRSA) Infection: Where Are We Now?. *J. Glob. Antimicrob Resist* **2**, 133–140;
659 <https://doi.org/10.1016/j.jgar.2014.03.009> (2014).
- 660 8. Bhatnagar, I. & Kim, S.K. Immense Essence of Excellence: Marine Microbial Bioactive
661 Compounds. *Mar Drugs* **8**, 2673–2701; <https://doi.org/10.3390/md8102673> (2010).

- 662 9. Bose, U. et al. LC-MS-Based Metabolomics Study of Marine Bacterial Secondary
663 Metabolite and Antibiotic Production in *Salinispora arenicola*. *Mar Drugs* **13**, 249–266;
664 <https://doi.org/10.3390/md13010249> (2015).
- 665 10. Stien, D. Marine Microbial Diversity as a Source of Bioactive Natural Products. *Mar Drugs*
666 **18**, 1-5; <https://doi.org/10.3390/md18040215> (2020).
- 667 11. Lane, A.L. & Moore, B.S. A Sea of Biosynthesis: Marine Natural Products Meet the
668 Molecular Age. *Nat Prod Rep.* **28**, 411–428; <https://doi.org/10.1039/C0NP90032J> (2011).
- 669 12. Blunt, J.W., Copp, B.R., Keyzers, R.A., Munro, M.H.G. & Prinsep, M.R. Marine Natural
670 Products. *Nat. Prod. Rep.* **30**, 144-222; <https://doi.org/10.1039/C2NP20112G> (2012).
- 671 13. Jose, P.A. & Jha, B. New Dimensions of Research on Actinomycetes: Quest for Next
672 Generation Antibiotics. *Front Microbiol* **7**, 1295;
673 <https://doi.org/10.3389/fmicb.2016.01295> (2016).
- 674 14. Hassan, S.S. & Shaikh, A.L. Marine Actinobacteria as a Drug Treasure House.
675 *Biomed Pharmacother* **87**, 46–57; <https://doi.org/10.1016/j.biopha.2016.12.086> (2017).
- 676 15. Lewis, K. The Science of Antibiotic Discovery. *Cell* **181**, 29-45;
677 <https://doi.org/10.1016/j.cell.2020.02.056> (2020).
- 678 16. Jose, P.A., Maharshi, A. & Jha. B. Actinobacteria in Natural Products Research: Progress
679 and Prospects. *Microbiol Res* **246**, 126708; <https://doi.org/10.1016/j.micres.2021.126708>
680 (2021).
- 681 17. Baltz, R. Renaissance in Antibacterial Discovery from Actinomycetes. *Curr Opin*
682 *Pharmacol* **8**, 557–563; <https://doi.org/10.1016/j.coph.2008.04.008> (2008).
- 683 18. Olano, C., Méndez, C. & Salas. A. Antitumor Compounds from Marine Actinomycetes.
684 *Mar Drugs* **7**, 210–248; <https://doi.org/10.3390/md7020210> (2009).
- 685 19. Bérdy, J. Bioactive Microbial Metabolites: A Personal View. *J Antibiot* **58**, 1–26;
686 <https://doi.org/10.1038/ja.2005.1> (2005).
- 687 20. Dettmer, K., Aronov, P.A. & Hammock, B.D. Mass Spectrometry-Based Metabolomics.
688 *Mass Spectrom Rev* **26**, 51–78; <https://doi.org/10.1002/mas.20108> (2007).
- 689 21. Gomez-Escribano, J.P., Alt, S. & Bibb, M. Next Generation Sequencing of
690 Actinobacteria for the Discovery of Novel Natural Products. *Mar Drugs* **14**, 78;
691 <https://doi.org/10.3390/md14040078> (2016).
- 692 22. Cornell, R.C., Marasini, D. & Mohamed F.K. Molecular Characterization of Plasmids
693 Harbored by Actinomycetes Isolated From the Great Salt Plains of Oklahoma Using PFGE

- 694 and Next Generation Whole Genome Sequencing. *Front Microbiol* **9**, 1-13;
695 <https://doi.org/10.3389/fmicb.2018.02282> (2018).
- 696 23. Hu, D. et al. Exploring the Potential of Antibiotic Production From Rare Actinobacteria by
697 Whole-Genome Sequencing and Guided MS/MS Analysis. *Front Microbiol* **11**, 1-12;
698 <https://doi.org/10.3389/fmicb.2020.01540> (2020).
- 699 24. Khoomrung, S. et al. Metabolomics and Integrative Omics for the Development of Thai
700 Traditional Medicine. *Front Pharmacol* **8**, 474; <https://doi.org/10.3389/fphar.2017.00474>
701 (2017).
- 702 25. Pye, C.R., Bertin, M.J., Lokey, R.S., Gerwick, W.H. & Linington, R.G. Retrospective
703 Analysis of Natural Products Provides Insights for Future Discovery Trends. *PNAS* **114**,
704 5601–5606; <https://doi.org/10.1073/pnas.1614680114> (2017).
- 705 26. Van der Hooft, J.J.J et al. Linking Genomics and Metabolomics to Chart Specialized
706 Metabolic Diversity. *Chem. Soc. Rev.* **49**, 3297–3314;
707 <https://doi.org/10.1039/D0CS00162G> (2020).
- 708 27. Caesar, L.K., Montaser, R., Keller, N.P. & Kelleher, N.L. Metabolomics and Genomics in
709 Natural Products Research: Complementary Tools for Targeting New Chemical Entities.
710 *Nat Prod Rep* **38**, 2041-2065; <https://doi.org/10.1039/D1NP00036E> (2021).
- 711 28. Macintyre, L. et al. Metabolomic Tools for Secondary Metabolite Discovery from Marine
712 Microbial Symbionts. *Mar Drugs* **12**, 3416–3448; <https://doi.org/10.3390/md12063416>
713 (2014).
- 714 29. Schneider, O. et al. Genome Mining of *Streptomyces* Sp. YIM 130001 Isolated From
715 Lichen Affords New Thiopeptide Antibiotic. *Front Microbiol* **9**, 1-12;
716 <https://doi.org/10.3389/fmicb.2018.03139> (2018).
- 717 30. Ye, Y. et al. Discovery of Three 22-Membered Macrolides by Deciphering the Streamlined
718 Genome of Mangrove-Derived *Streptomyces* Sp. HM190. *Front Microbiol* **11**, 1-13;
719 <https://doi.org/10.3389/fmicb.2020.01464> (2020).
- 720 31. Liu, X. & Locasale, J.W. Metabolomics: A Primer. *Trends Biochem Sci* **42**, 274-284;
721 <https://doi.org/10.1016/j.tibs.2017.01.004> (2017).
- 722 32. Wang, M. et al. Sharing and Community Curation of Mass Spectrometry Data with Global
723 Natural Products Social Molecular Networking. *Nat. Biotechnol* **34**, 828–837;
724 <https://doi.org/10.1038/nbt.3597> (2016).
- 725 33. Palazzotto, E., Tong, Y., Lee, S.Y. & Weber, T. Synthetic Biology and Metabolic
726 Engineering of Actinomycetes for Natural Product Discovery. *Biotechnol Adv* **37**, 1-15;
727 <https://doi.org/10.1016/j.biotechadv.2019.03.005> (2019).

- 728 34. Shang, Z. et al. Grincamycins P–T: Rearranged Angucyclines from the Marine Sediment-
729 Derived *Streptomyces* Sp. CNZ-748 Inhibit Cell Lines of the Rare Cancer Pseudomyxoma
730 Peritonei. *J Nat Prod* **84**, 1638–1648; <https://doi.org/10.1021/acs.jnatprod.1c00179> (2021).
- 731 35. Maskey, R.P., Helmke, E. & Laatsch, H. Himalomycin A and B: isolation and structure
732 elucidation of new fridamycin type antibiotics from a marine *Streptomyces* isolate. *J*
733 *Antibiot* **56**, 942-949; <https://doi: 10.7164/antibiotics.56.942>. PMID: 14763560 (2003).
- 734 36. Alvi, A.A., Baker, D.D., Stienecker, V., Hosken, M. & Nair, B.G. Identification of
735 Inhibitors of Inducible Nitric Oxide Synthase from Microbial Extracts. *J Antibiot* **53**, 496–
736 501; <https://doi.org/10.7164/antibiotics.53.496> (2000).
- 737 37. Song, Y. et al. Cytotoxic and Antibacterial Angucycline- and Prodigiosin- Analogues from
738 the Deep-Sea Derived *Streptomyces* Sp. SCSIO 11594. *Mar Drugs* **13**, 1304–1316;
739 <https://doi.org/10.3390/md13031304> (2015).
- 740 38. Zhu, X. et al. Cytotoxic Rearranged Angucycline Glycosides from Deep Sea-Derived
741 *Streptomyces Lusitanus* SCSIO LR32. *J Antibiot* **70**, 819–822;
742 <https://doi.org/10.1038/ja.2017.17> (2017).
- 743 39. Rix, U., Rensing, L.L, Hoffmeister, D., Bechthold, A. & Rohr, J. Urdamycin L: A Novel
744 Metabolic Shunt Product That Provides Evidence for the Role of the UrdM Gene in the
745 Urdamycin A Biosynthetic Pathway of *Streptomyces Fradiae* Tü 2717. *ChemBioChem* **4**,
746 109–911; <https://doi.org/10.1002/cbic.200390002> (2003).
- 747 40. Imamura, N., Kakinuma, K., Ikekawa, N., Tanaka, H. & Omura S. Biosynthesis of
748 vineomycins A1 and B2. *J Antibiot* **35**, 602-608; <https://doi: 10.7164/antibiotics.35.602>
749 (1982).
- 750 41. Bao, J et al. Cytotoxic Antibiotic Angucyclines and Actinomycins from the *Streptomyces*
751 Sp. XZHG99T. *J Antibiot* **71**, 1018–1024; <https://doi.org/10.1038/s41429-018-0096-1>
752 (2018).
- 753 42. Tan, B. et al. Identification of Endogenous Acyl Amino Acids Based on a Targeted
754 Lipidomics Approach. *J Lipid Res* **51**, 112–219; [https://doi.org/10.1194/jlr.M900198-
755 JLR200](https://doi.org/10.1194/jlr.M900198-JLR200) (2010).
- 756 43. Nakagawa, K., Hara, C., Tokuyama, S. Takada, K. & Imamura, I. Saprolymycins A–E, New
757 Angucycline Antibiotics Active against *Saprolegnia Parasitica*. *J Antibiot* **65**, 599–607;
758 <https://doi.org/10.1038/ja.2012.86> (2012).

- 759 44. Zhang, Y. et al. Identification of the Grincamycin Gene Cluster Unveils Divergent Roles
760 for GcnQ in Different Hosts, Tailoring the L -Rhodinose Moiety. *Org Lett* **15**, 3254–3257;
761 <https://doi.org/10.1021/ol401253p> (2013).
- 762 45. Seemann, T. Prokka: Rapid Prokaryotic Genome Annotation. *Bioinform* **30**, 2068–2069;
763 <https://doi.org/10.1093/bioinformatics/btu153> (2014).
- 764 46. Peng, A. et al. Angucycline Glycosides from an Intertidal Sediments Strain *Streptomyces*
765 sp. and Their Cytotoxic Activity against Hepatoma Carcinoma Cells. *Mar Drugs* **16**, 1-10;
766 <https://doi.org/10.3390/md16120470> (2018).
- 767 47. Hu, Z. et al. Angucycline Antibiotics and Its Derivatives from Marine-Derived
768 Actinomycete *Streptomyces* Sp. A6H. *Nat Prod Res* **30**, 2551–2558;
769 <https://doi.org/10.1080/14786419.2015.1120730> (2016).
- 770 48. Rohr, J. & Thiericke, R. Angucycline Group Antibiotics. *Nat Prod Rep* **9**, 103-137;
771 <https://doi.org/10.1039/np9920900103> (1992).
- 772 49. Kharel, M.k. et al. Angucyclines: Biosynthesis, Mode-of-Action, New Natural Products,
773 and Synthesis. *Nat Prod Rep* **29**, 264–325; <https://doi.org/10.1039/C1NP00068C> (2012).
- 774 50. Fürst, M.J. L. J., Gran-Scheuch, A., Aalbers, F.S & Fraaije. M.W. Baeyer–Villiger
775 Monooxygenases: Tunable Oxidative Biocatalysts. *ACS Catal* **9**, 11207–11241.
776 <https://doi.org/10.1021/acscatal.9b03396> (2019).
- 777 51. Laslett, D. & Canback, B. ARAGORN, a Program to Detect tRNA Genes and tmRNA
778 Genes in Nucleotide Sequences. *Nucleic Acids Res* **32**, 11–16;
779 <https://doi.org/10.1093/nar/gkh152> (2004).
- 780 52. Gruber, A. R., Lorenz, R., Bernhart, S., Neubock, R. & Hofacker, I.L. The Vienna RNA
781 Websuite. *Nucleic Acids Res* **36**, 70–74; <https://doi.org/10.1093/nar/gkn188> (2008).
- 782 53. Faust, B et al. Two New Tailoring Enzymes, a Glycosyltransferase and an Oxygenase,
783 Involved in Biosynthesis of the Angucycline Antibiotic Urdamycin A in *Streptomyces*
784 *fradiae* Tu\$ 2717. *Microbiology* **146**, 147-154; <https://doi.org/10.1099/00221287-146-1-147>
785 (2000).
- 786 54. Decker, H. & Haag, S. Cloning and Characterization of a Polyketide Synthase Gene from
787 *Streptomyces fradiae* Tü2717, Which Carries the Genes for Biosynthesis of the
788 Angucycline Antibiotic Urdamycin A and a Gene Probably Involved in Its Oxygenation. *J*
789 *Bacteriol* **177**, 6126–6136; <https://doi.org/10.1128/jb.177.21.6126-6136.1995> (1995).
- 790 55. Rix, U., Fischer, C., Remsing, L.L. & Rohr, J. Modification of Post-PKS Tailoring Steps
791 through Combinatorial Biosynthesis. *Nat Prod Rep* **19**, 542–580;
792 <https://doi.org/10.1039/b103920m> (2002).

- 793 56. Guo, F. *et al.* Targeted activation of silent natural product biosynthesis pathways by
794 reporter-guided mutant selection. *Metab Eng* **28**, 134–142;
795 <http://dx.doi.org/10.1016/j.ymben.2014.12.006> (2015).
- 796 57. Kallio, P. *et al.* Flavoprotein Hydroxylase PgaE Catalyzes Two Consecutive Oxygen-
797 Dependent Tailoring Reactions in Angucycline Biosynthesis. *Biochemistry* **50**, 5535–5543;
798 <http://dx.doi.org/10.1021/bi200600k> (2011).
- 799 58. Du, Y. *et al.* Identification and Characterization of the Biosynthetic Gene Cluster of
800 Polyoxypeptin A, a Potent Apoptosis Inducer. *BMC Microbiol* **14**, 30;
801 <https://doi.org/10.1186/1471-2180-14-30> (2014)
- 802 59. Salem, S. M., Weidenbach, S. & Rohr, J. Two Cooperative Glycosyltransferases Are
803 Responsible for the Sugar Diversity of Saquayamycins Isolated from *Streptomyces* sp. KY
804 40-1. *ACS Chem. Biol.* **12**, 2529–2534 (2017).
- 805 60. Kawasaki, T., Moriyama, A., Nakagawa, K. & Imamura, N. Cloning and Identification of
806 Saprolmycin Biosynthetic Gene Cluster from *Streptomyces* Sp. TK08046.
807 *Biosci Biotechnol Biochem* **80**, 2144–2150;
808 <https://doi.org/10.1080/09168451.2016.1196574> (2016).
- 809 61. Basnet, D.B. *et al.* Angucyclines Sch 47554 and Sch 47555 from *Streptomyces* Sp. SCC-
810 2136: Cloning, Sequencing, and Characterization. *Mol Cells* **9**, 154–162 (2006).
- 811 62. Mittler, M., Bechthold, A. & Schulz, G.E. Structure and Action of the C–C Bond-Forming
812 Glycosyltransferase UrdGT2 Involved in the Biosynthesis of the Antibiotic Urdamycin. *J*
813 *Mol Biol* **372**, 67–76; <https://doi.org/10.1016/j.jmb.2007.06.005> (2007).
- 814 63. Fidan, O. *et al.* New Insights into the Glycosylation Steps in the Biosynthesis of Sch47554
815 and Sch47555. *ChemBioChem* **19**, 1424–1432; <https://doi.org/10.1002/cbic.201800105>
816 (2018).
- 817 64. Elshahawi, S.I., Shaaban, K.K., Kharel, M.K. & Thorson, J.S. A Comprehensive Review
818 of Glycosylated Bacterial Natural Products. *Chem Soc Rev* **44**, 7591–7697;
819 <https://doi.org/10.1039/C4CS00426D> (2015).
- 820 65. Myronovskiy, M. *et al.* Generation of New Compounds through Unbalanced Transcription
821 of Landomycin A Cluster. *Appl Microbiol Biotechnol* **100**, 9175–9186;
822 <https://doi.org/10.1007/s00253-016-7721-3> (2016).
- 823 66. Tawfike, A. *et al.* New Bioactive Metabolites from the Elicited Marine Sponge-Derived
824 Bacterium *Actinokineospora Spheciospongiae* sp. Nov. *AMB Expr* **9**, 1–9;
825 <https://doi.org/10.1186/s13568-018-0730-0> (2019).

- 826 67. Keller, U, Lang, M., Crnovcic, I., Pfennig, F., & Schauwecker, F. The Actinomycin
827 Biosynthetic Gene Cluster of *Streptomyces Chrysomallus*: A Genetic Hall of Mirrors for
828 Synthesis of a Molecule with Mirror Symmetry. *J Bacteriol* **192**, 2583–2595;
829 <https://doi.org/10.1128/JB.01526-09> (2010).
- 830 68. Hubbard, B.K., Thomas, M.G. & Walsh, C.T. Biosynthesis of L-p-Hydroxyphenylglycine,
831 a Non-Proteinogenic Amino Acid Constituent of Peptide Antibiotics. *Chem Biol* **7**, 931-
832 941; [https://doi: 10.1016/s1074-5521\(00\)00043-0](https://doi.org/10.1016/s1074-5521(00)00043-0) (2000).
- 833 69. Cobb, R. E., Wang, Y. & Zhao, H. High-Efficiency Multiplex Genome Editing of
834 *Streptomyces* Species Using an Engineered CRISPR/Cas System. *ACS Synth. Biol.* **4**, 723–
835 728; [https://doi: 10.1021/sb500351f](https://doi.org/10.1021/sb500351f) (2015).
- 836 70. Tong, Y. *et al.* CRISPR–Cas9, CRISPRi and CRISPR-BEST-mediated genetic
837 manipulation in streptomycetes. *Nat Protoc* **15**, 2470–2502 (2020).
- 838 71. Hirsch, C F. & Christensen, D.L. Novel Method for Selective Isolation of Actinomycetes.
839 *Appl Environ Microbiol* **46**, 925–929; <https://doi.org/10.1128/aem.46.4.925-929.1983>
840 (1983).
- 841 72. Jensen, P.R., Dwight, R. & Fenical, W. Distribution of Actinomycetes in Near-Shore
842 Tropical Marine Sediments. *Appl Environ Microbiol* **57**, 1102–1108;
843 <https://doi.org/10.1128/AEM.57.4.1102-1108.1991> (1991).
- 844 73. Shirling, E. B. & Gottlieb, D. Methods for Characterization of *Streptomyces* Species. *Int J*
845 *Syst. Bacteriol* **16**, 313–340; <https://doi.org/10.1099/00207713-16-3-313> (1966).
- 846 74. Fagervold, S. K. *et al.* *Pleionea Mediterranea* Gen. Nov., Sp. Nov., a
847 Gammaproteobacterium Isolated from Coastal Seawater. *Int. J. Syst. Evol* **63**, 2700–2705;
848 <https://doi.org/10.1099/ijms.0.045575-0> (2013).
- 849 75. Yoon, S. H *et al.* Introducing EzBioCloud: A Taxonomically United Database of 16S
850 rRNA Gene Sequences and Whole-Genome Assemblies. *Int J Syst Evol.* **67**, 1613–1617;
851 <https://doi.org/10.1099/ijsem.0.001755> (2017).
- 852 76. Shomura, T. *et al.* Studies on Actinomycetales producing antibiotics only on agar culture.
853 I. Screening, taxonomy and morphology-productivity relationship of *Streptomyces*
854 *halstedii*, strain SF-1993. *J Antibiot* **32**, 427-435; [https://doi: 10.7164/antibiotics.32.427](https://doi.org/10.7164/antibiotics.32.427)
855 (1979).
- 856 77. Nkanga, E.J. & Hagedorn, C. Detection of Antibiotic-Producing *Streptomyces* Inhabiting
857 Forest Soils. *Antimicrob. Agents Chemother* **14**, 51-59;
858 <https://doi.org/10.1128/AAC.14.1.51> (1978).

- 859 78. CLSI: Clinical and Laboratory Standards Institute: Performance standards for antimicrobial
860 susceptibility testing; Twenty-sixth informational supplement. CLSI document M100-S26.
861 Wayne, PA: Clinical and Laboratory Standards Institute (2016).
- 862 79. Stien, D. et al. Metabolomics Reveal That Octocrylene Accumulates in *Pocillopora*
863 *Damicornis* Tissues as Fatty Acid Conjugates and Triggers Coral Cell Mitochondrial
864 Dysfunction. *Anal Chem* **91**, 990–995; <https://doi.org/10.1021/acs.analchem.8b04187>
865 (2019).
- 866 80. Stien, D. A Unique Approach to Monitor Stress in Coral Exposed to Emerging Pollutants.
867 *Sci Rep* **10**, 1-11; <https://doi.org/10.1038/s41598-020-66117-3> (2020).
- 868 81. Otasek, D., Morris, J.H., Bouças, Pico, A.R. & Demchak, D. Cytoscape Automation:
869 Empowering Workflow-Based Network Analysis. *Genome Biol* **20**, 1-15;
870 <https://doi.org/10.1186/s13059-019-1758-4> (2019).
- 871 82. Dührkop, K. SIRIUS 4: A Rapid Tool for Turning Tandem Mass Spectra into Metabolite
872 Structure Information. *Nat Methods* **16**, 299–302; [https://doi.org/10.1038/s41592-019-](https://doi.org/10.1038/s41592-019-0344-8)
873 [0344-8](https://doi.org/10.1038/s41592-019-0344-8) (2019).
- 874 83. Ruttkies, C., Schymanski, E.L., Wolf, W., Hollender, J. & Neumann, S. MetFrag
875 Relunched: Incorporating Strategies beyond in Silico Fragmentation. *J Cheminform* **8**, 1-
876 16; <https://doi.org/10.1186/s13321-016-0115-9> (2016).
- 877 84. Prjibelski, A., Antipov, D., Meleshko, D., Lapidus, A. & Korobeynikov, A. Using SPAdes
878 De Novo Assembler. *Curr Protoc Bioinform* **70**, 1-29; <https://doi.org/10.1002/cpbi.102>
879 (2020).
- 880 85. Antony-Babu. S et al. Multiple *Streptomyces* Species with Distinct Secondary
881 Metabolomes Have Identical 16S rRNA Gene Sequences. *Sci Rep* **7**, 11089;
882 <https://doi.org/10.1038/s41598-017-11363-1> (2017).
- 883 86. Blin, K. et al. AntiSMASH 6.0: Improving Cluster Detection and Comparison Capabilities.
884 *Nucleic Acids Res* **49**, 29–35; <https://doi.org/10.1093/nar/gkab335> (2021).
- 885 87. Gilchrist, C.L.M. & Chooi, Y.H. clinker & clustermap.js: automatic generation of gene
886 cluster comparison figures. *Bioinformatics* **37**, 2473–2475; [https://doi:](https://doi.org/10.1093/bioinformatics/btab007)
887 [10.1093/bioinformatics/btab007](https://doi.org/10.1093/bioinformatics/btab007) (2021).
- 888 88. Gouy, M., Guindon, S. & Gascuel, O. SeaView Version 4: A Multiplatform Graphical User
889 Interface for Sequence Alignment and Phylogenetic Tree Building. *Mol Biol Evol* **27**, 221–
890 224; <https://doi.org/10.1093/molbev/msp259> (2010).

891

892

893 **Acknowledgements**

894 We thank the Bio2Mar platform (<http://bio2mar.obs-banyuls.fr>) for providing technical support
895 and access to instrumentation. This work benefited from access to the Observatoire
896 Océanologique de Banyuls-sur-Mer, an EMBRC-France and EMBRC-ERIC site.

897 **Author Contributions:** R.O., D.S, and M.S. conceived and designed the experiments. R.O.
898 and K.M. collected biological material. R.O., A.S.R., C.V. performed the experiments. D.S.
899 and J.S. performed the metabolomics analysis. R.O and M.T.S the genomic analysis. R.O., D.S.,
900 and M.T.S. wrote the original draft and prepared tables and figures. All authors read and
901 approved the final version.

902 **Additional Information**

903 **Data availability:** The draft genome sequence was deposited in the GenBank database under
904 accession number JAJQKZ000000000. Raw Illumina reads have been deposited in the SRA
905 under accession SRR17084181. The sequence analysis pipeline plus discussions regarding
906 angucycline biosynthesis, AntiSMASH results and the files used for the phylogenetic analysis
907 are available through are available through github (github.com/suzumar/ROS4_manus).

908
909 **Funding:** This work was funded by recurrent funds of the CNRS and Sorbonne University
910 attributed to the LBBM laboratory.

911 **Competing interests:** The authors declare no conflicts of interest.

912

913

914